JCTC Journal of Chemical Theory and Computation

Parameter Calibration of Transition-Metal Elements for the Spin-Polarized Self-Consistent-Charge Density-Functional Tight-Binding (DFTB) Method: Sc, Ti, Fe, Co, and Ni

Guishan Zheng,[†] Henryk A. Witek,[‡] Petia Bobadova-Parvanova, Stephan Irle,[§] Djamaladdin G. Musaev, Rajeev Prabhakar,[||] and Keiji Morokuma*

Department of Chemistry and Cherry L. Emerson Center for Scientific Computation, Emory University, Atlanta, Georgia 30322

Marcus Lundberg

Fukui Institute for Fundamental Chemistry, Kyoto University, Sakyo, Kyoto 606-8103, Japan

Marcus Elstner,[⊥] Christof Köhler,[#] and Thomas Frauenheim[#]

Universität Paderborn, Fachbereich Physik, 33095 Paderborn, Germany

Received October 24, 2006

Abstract: Recently developed parameters for five first-row transition-metal elements (M = Sc, Ti, Fe, Co, and Ni) in combination with H, C, N, and O as well as the same metal (M−M) for the spin-polarized self-consistent-charge density-functional tight-binding (DFTB) method have been calibrated. To test their performance a couple sets of compounds have been selected to represent a variety of interactions and bonding schemes that occur frequently in transition-metal containing systems. The results show that the DFTB method with the present parameters in most cases reproduces structural properties very well, but the bond energies and the relative energies of different spin states only qualitatively compared to the B3LYP/SDD+6-31G(d) density functional (DFT) results. An application to the ONIOM(DFT:DFTB) indicates that DFTB works well as the low level method for the ONIOM calculation.

1. Introduction

Molecules that contain transition-metal atoms play an important role in catalysis, material science, drug design, and enzymatic reactions. Theoretical modeling of such systems is challenging due to their large size and complexity of their electronic structure arising from the presence of chemically active d-electrons. Despite the advent of fast computers and advanced techniques, high level ab initio methods are prohibitively expensive to treat very large molecular systems. A partial remedy for this problem can be the density functional theory (DFT),[1−3] which can be used routinely to systems containing a few hundred atoms with the present computers.

Efforts to reduce computational cost associated with quantum chemical calculations have led in last several decades to development of a large number of semiempirical methods, such as MNDO,[4,5] SINDO/1,[6,7] AM1,[8] PM3,[9,10] SAM1,[11,12] MNDO/d,[13,14] PM3/tm,[15] NDDO-G,[16] PDDG/PM3,[17−20] NO-MNDO,[21] and RM1[22] which can routinely

* Corresponding author e-mail:morokuma@emory.edu. Also at Fukui Institute for Fundamental Chemistry, Kyoto University, Kyoto, Japan.

[†] Present address: Department of Chemistry, University of Illinois, Urbana, IL 61801.

[‡] Present address: Institute of Molecular Science and Department of Applied Chemistry, National Chiao Tung University, Hsinchu, Taiwan.

[§] Present address: Institute for Advanced Research and Department of Chemistry, Nagoya University, Nagoya 464-8602, Japan.

[||] Present address: Department of Chemistry, University of Miami, Coral Gables, FL 33124.

[⊥] Present address: Technical University, Braunschweig, Germany.

[#] Present address: University of Bremen, Bremen, Germany.

10.1021/ct600312f CCC: $37.00
Published on Web 06/05/2007

treat molecular systems containing up to 1000 or so atoms. An alternative approach to perform calculations for such large systems is an approximate density functional technique called the density functional tight-binding (DFTB) method.[23,24] This method has been applied to calculating energies, geometries, and spectra of organic and inorganic molecules.[23−29] The accuracy for molecular geometries is comparable to that of DFT-GGA methods, while reaction energies and vibrational frequencies are slightly less accurate.[20,25,30−36] Recently, a special parametrization for vibrational frequencies has shown that DFTB can approach the DFT accuracy,[37] while heats of formation are still slightly less accurate than those determined at recently optimized MNDO approaches.[21]

In the present article, we will use a specific version of the series of DFTB methods, the spin-polarized self-consistent charge DFTB,[38] which is based on a second-order expansion of the Kohn−Sham total energy with respect to spin densities. This method introduces a self-consistent calculation of the spin density using Mulliken populations. The SCF procedure minimizes the dependence of the results on the choice of the zero-order initial density and substantially increases the transferability of the parameters in comparison with the non-self-consistent-charge approach.[24] In addition, the spin-polarized version of DFTB distinguishes different spin distributions (whereas spin-unpolarized DFTB depends only on the total electron density) and can qualitatively describe different spin states, a fact that is essential for transition-metal elements. All the needed one- and two-center integrals are precomputed for a large number of grid points, and, in practical calculations, the actual values of integrals are obtained by a suitable interpolation scheme, usually a cubic spline function fitting. All electronic parameters of the spin-polarized DFTB model are calculated from DFT using the PBE functional,[39] while two-center repulsive potentials are fitted to results using hybrid functional, i.e., B3LYP;[40,41] no fitting to experimental data is involved. Since only valence electrons are considered in a minimal basis set and explicit integral evaluations are not required, DFTB is computationally comparable to semiempirical methods (like MNDO, AM1, PM3) and 2−3 orders of magnitude faster than ab initio Hartree−Fock (HF) and density functional theory (DFT) methods.[25] As a result, the computational speed of DFTB is determined to a large extent by the solution of the generalized eigenvalue problem.

Up to now, the only transition metals available in DFTB are Zn[26] and some other scattered atom pair parameters,[27,42−58] and therefore one of the serious drawbacks of the DFTB method was the lack of parameters for further transition-metal elements, which play an important role in many inorganic, organometallic, and metalloprotein problems. This situation has restricted the active use of DFTB methods from many interesting applications.

In the present paper, we present our recent work on extending the currently available spin-polarized DFTB parameter database in the form of the Paderborn group to five additional elements: Sc, Ti, Fe, Co, and Ni, which are parametrized in combination with C, H, O, and N nonmetal elements as well as with the element itself (dimer). In section 2, we give an overview and procedure for the parametrization procedure. In section 3, test calculations using the new parameters are discussed and analyzed. Here, the performance of the parameter sets in different chemical environments is discussed in detail, focusing on calculated molecular geometries and energies. In section 3, we present a sample application of the new parameters in ONIOM(DFT:DFTB) method, and in section 4, we summarize the performance and problems of the new parameters.

2. Method and Parametrization

A. Spin-Polarized Self-Consistent-Charge DFTB Approach. A detailed description of the spin-polarized self-consistent-charge density-functional tight-binding (DFTB) method has been given elsewhere.[38,59,60] Here a brief review is presented. The total spin-polarized DFTB energy is given by

$$E_{\mathrm{tot}}^{\mathrm{SDFTB}} = \sum_{\sigma=\uparrow,\downarrow}\sum_{i}^{\mathrm{MO}} n_i^{\sigma}\langle\psi_i^{\sigma}|\hat{H}^0[\rho_0]|\psi_i^{\sigma}\rangle + \frac{1}{2}\sum_{A,B}^{\mathrm{atom}} \gamma_{AB}\Delta q_A \Delta q_B + \frac{1}{2}\sum_{A}^{\mathrm{atom}}\sum_{l}\sum_{l'} p_{Al}\, p_{Al'} W_{All'} + E^{\mathrm{rep}} \quad (1)$$

where $\uparrow$ and $\downarrow$ denote the up and down spin orientation, γ_{AB} is a distance-dependent interaction parameter between induced Mulliken charges Δq_{A}, Δq_{B} on atoms A and B, $W_{All'}$ is a one-center interaction parameter between the l and l' shell spin densities p_{Al}, $p_{Al'}$ on atom A, E_{rep} is a sum of two-center core−core repulsive potentials:

$$E^{\mathrm{rep}} = \sum_{A<B}^{\mathrm{atom}} E_{AB}^{\mathrm{rep}} \quad (2)$$

and n_i^{σ} is the occupation number of the spin orbital ψ_i^{σ} that is given as a linear combination of localized pseudoatomic Slater orbitals χ_μ

$$\psi_i^{\sigma} = \sum_{\mu}^{\mathrm{AO}} c_{\mu i}^{\sigma}\chi_\mu \quad (3)$$

The induced Mulliken charge Δq_A on atom A is given by

$$\Delta q_A = \sum_{i}^{\mathrm{MO}}\sum_{\mu\in A}\sum_{\nu}^{\mathrm{AO}} (n_i^{\uparrow} c_{\mu i}^{\uparrow} c_{\nu i}^{\uparrow} + n_i^{\downarrow} c_{\mu i}^{\downarrow} c_{\nu i}^{\downarrow}) S_{\mu\nu} - q_A^0 \quad (4)$$

and the spin density p_{Al} of shell l on atom A is given by

$$p_{Al} = \sum_{i}^{\mathrm{MO}}\sum_{\mu\in l}\sum_{\nu}^{\mathrm{AO}} (n_i^{\uparrow} c_{\mu i}^{\uparrow} c_{\nu i}^{\uparrow} - n_i^{\downarrow} c_{\mu i}^{\downarrow} c_{\nu i}^{\downarrow}) S_{\mu\nu} \quad (5)$$

where S is the overlap matrix of pseudoatomic Slater orbitals, and q_A^0 is the valence charge on the neutral atom A. The effective Kohn−Sham Hamiltonian $\hat{H}^0$ depends only on the reference density ρ_0.

The derivation of the spin-polarized DFTB energy with respect to nuclear coordinate a yields the DFTB energy gradient acting on atom A. The exact formula and its derivation can be found elsewhere.[60]

Table 1. Chemical Hardness or Hubbard Parameters U_{Ml} and the Atomic Spin-Dependent Constants $W_{Mll'}$ (both in Hartree) for M = Sc, Ti, Fe, Co, and Ni

element	Sc	Ti	Fe	Co	Ni
U_s	0.18881	0.20020	0.20050	0.26064	0.23145
U_p	0.13784	0.14432	0.20050	0.11593	0.18913
U_d	0.32717	0.35522	0.36342	0.38599	0.40632
W_{ss}	−0.013	−0.014	−0.016	−0.016	−0.016
W_{sp}	−0.011	−0.012	−0.012	−0.012	−0.012
W_{sd}	−0.005	−0.004	−0.003	−0.003	−0.003
W_{pp}	−0.014	−0.014	−0.029	−0.033	−0.022
W_{pd}	−0.002	−0.001	−0.001	−0.001	−0.001
W_{dd}	−0.013	−0.014	−0.015	−0.016	−0.018

B. Development of Atomic and Diatomic Parameters Sets. We develop the M−M and M−X diatomic parameter sets, where M = Sc, Ti, Fe, Co, and Ni and X = H, C, O, and N. Atomic valence orbitals are obtained by solving an all-electron Kohn−Sham atomic eigenvalue problem with an additional confining potential. The repulsive potentials for each pair of atoms are obtained by reproducing DFT energies and geometries for a number of carefully selected molecular systems; their choice is ideally meant to represent the most important chemical compounds created by a given pair of atoms.

In the present paper, spin-polarized DFTB parametrization is performed in the same way as in the standard, nonspin-polarized self-consistent-charge (SCC-) method.[61] Here, we will review briefly the main ideas of the parametrization procedure together with necessary modifications required by the introduction of the spin-polarization term. There are two families of parameters necessary to construct the spin-polarized DFTB Hamiltonian, namely (1) atomic parameters obtained from calculations for confined pseudoatoms and (2) diatomic distance-dependent parameters obtained from diatomic calculations.

Atomic Parameters. The required spin-polarized DFTB atomic parameters comprise atomic basis functions χ_μ, chemical hardness or Hubbard parameters U_{Al}, and the atomic spin-dependent constants $W_{All'}$. U_{Al} is determined by taking the second derivative of the total atomic energy with respect to the total charge on orbital l of atom A. The values of $W_{All'}$ are calculated by taking the second derivatives of the total atomic energy with respect to the spin density; at the point where the spin density is zero, this derivative reduces to[38]

$$W_{All'} = \frac{1}{2}\left(\frac{\partial \epsilon_{Al}^{\uparrow}}{\partial n_{l'}^{\uparrow}} - \frac{\epsilon_{Al}^{\uparrow}}{\partial n_{l'}^{\downarrow}}\right)_{\rho=0} = W_{Al'l} \qquad (6)$$

where n_l and $n_{l'}$ are the occupation numbers of atomic shells l and l', respectively, and $\epsilon_{Al}^{\uparrow}$ is the atomic Kohn−Sham orbital energy for alpha (↑) spin. The second derivative values are computed using finite difference method. The determined values of U_{Al} and $W_{All'}$ are listed in Table 1 for all the considered metal elements.

We use a standard procedure to construct the atomic basis set. It is expressed as a linear combination of Slater spherical harmonics; the coefficients are obtained from atomic Kohn−Sham calculations with the PBE functional[39] and an additional confining potential $(r/r_0)^2$ (in Hartree). The confinement mimics the behavior of atoms in molecular systems and in solids. The values of r_0 (4.86 for Sc, 3.6 for Ti, 3.2 for Fe, 4.38 for Co, and 3.2 for Ni, all in bohr) have been selected out of a large number of trials and ensure that SCC-DFTB reproduces accurate DFT electronic band structures for solid-state metals to the highest possible degree.

Diatomic Parameters. The overlap $S_{\mu\nu}$ and Hamiltonian $H^0_{\mu\nu}$ matrix elements are obtained from two-center approximate noniterative DFT calculations on the corresponding diatomic compounds for a large number of different interatomic distances, i.e., the two-center integral calculations using atomic wavefunctions from previous pseudoatomic calculations. The term "approximate DFT" refers to the fact that the exchange-correlation functional is built from approximate electronic density obtained as a simple sum of unperturbed atomic densities. The atomic densities for these transition-metal atoms are obtained from an auxiliary pseudoatomic calculation with an additional confining potential (r/r_0),[2] where a universal value of $r_0 = 14$ bohr is adopted for all studied transition metals. It is important to stress that the confinement radius r_0 used previously to construct valence atomic orbitals is different from the confinement radius used here to generate the zero-order unperturbed atomic density. The confinement radius for the orbitals is used to generate a minimal LCAO basis set that is appropriate for the target molecular systems, i.e., the choice of this parameter for the basis set determination can be compared to the procedure of basis set construction for HF or DFT calculations and r_0 has originally been treated as a variational parameter.[62] The choice of the confinement radius for the density is different in its nature; it can be interpreted as an empirical value to generate an optimal starting (input) density that is characteristic to tight-binding methods.[63]

These two confinement radii can be treated as parameters used to enhance the performance of new DFTB parameter sets. However, the influence of these values on molecular properties is rather small. In the present parametrization procedure the PBE functional is used.[39] The orbitals employed in this calculation are atomic Slater orbitals with confined potential discussed in the paragraph above. The values of $S_{\mu\nu}$ and $H^0_{\mu\nu}$ are represented numerically on a grid of atomic distance.

Determination of the two-center repulsive potentials E_{AB}^{rep} is the most labor-intensive and therefore most time-consuming step in the parametrization procedure. The repulsive potential function is the difference between the DFT energy and the DFTB electronic energy as a function of atomic distance. At first, segments of each repulsion potential were calculated for a carefully selected group of molecules (called tier 1 molecules in Table 2) representing a large spectrum of bonding situations (covalent single and multiple bonds, ionic bonds, back-donation bonds, π-interactions, etc.) for a given pair of elements A-B. We have used small molecules containing only a few atoms, in which typically additional hydrogen or other atoms have been used to saturate the unfilled valences of given transition-metal and nonmetal atoms. In general, mainly closed-shell molecules have been

Table 2. List of Molecules and Their Spin States Used in the Parametrization Procedure[a]

	M−M	M−H	M−C	M−N	M−O
			M = Sc		
tier 1	$^1Sc_2$	$^1ScH_3$	$^1HScCH_2$	^1ScN	^1HScO
			$^1H_2ScCH_3$	$^1H_2ScN_2$	$^1H_2ScOH$
			M = Ti		
tier 1	$^1Ti_2$	$^1TiH2$	^1HTiCH	^1HTiN	^1H_2TiO
			$^1H_2TiCH_2$	$^1H_2TiNH$	$^1H_3TiOH$
			$^1H_3TiCH_3$	$^1H_3TiNH_2$	
tier 2			$^1Ti(CO)_2^{+4}$	$^1Ti(NH_3)_2^{+4}$	$^1Ti(H_2O)_2^{+4}$
			$^1Ti(CO)_3^{+4}$	$^1Ti(NH_3)_3^{+4}$	$^1Ti(H_2O)_3^{+4}$
			$^1Ti(CO)_4^{+4}$	$^1Ti(NH_3)_4^{+4}$	$^1Ti(H_2O)_4^{+4}$
			$^1Ti(CO)_5^{+4}$	$^1Ti(NH_3)_5^{+4}$	$^1Ti(H_2O)_5^{+4}$
			$^1Ti(CO)_6^{+4}$	$^1Ti(NH_3)_6^{+4}$	$^1Ti(H_2O)_6^{+4}$
			M = Fe		
tier 1	$^1Fe_2$	$^1FeH_2$	$^1FeCH_2$	^1FeNH	^1FeO
			$^1FeCH_3^+$	$^1HFeNH_2$	^1HFeOH
			^1HFeCO	$^1FeNH_3^{+2}$	$^1FeOH_2^{+2}$
tier 2			$^6Fe(CO)_2^{+3}$	$^6Fe(NH_3)_2^{+3}$	$^6Fe(H_2O)_2^{+3}$
			$^6Fe(CO)_3^{+3}$	$^6Fe(NH_3)_3^{+3}$	$^6Fe(H_2O)_3^{+3}$
			$^6Fe(CO)_4^{+3}$	$^6Fe(NH_3)_4^{+3}$	$^6Fe(H_2O)_4^{+3}$
			$^6Fe(CO)_5^{+3}$	$^6Fe(NH_3)_5^{+3}$	$^6Fe(H_2O)_5^{+3}$
			$^6Fe(CO)_6^{+3}$	$^6Fe(NH_3)_6^{+3}$	$^6Fe(H_2O)_6^{+3}$
			M = Co		
tier 1	$^1Co_2$	$^2CoH_2$	^1CoCH	^1CoN	^1HCoO
		$^1CoH_3$	$^2CoCH_2^+$	^1HCoNH	$^1HOCoH_2$
			$^2CoCO^{2+}$	$^2CoNH_3^{+2}$	
tier 2			$^2Co(CO)_1^{+2}$	$^2Co(NH_3)_1^{+2}$	$^2Co(H_2O)_1^{+2}$
			$^2Co(CO)_2^{+2}$	$^2Co(NH_3)_2^{+2}$	$^2Co(H_2O)_2^{+2}$
			$^2Co(CO)_3^{+2}$	$^2Co(NH_3)_3^{+2}$	$^2Co(H_2O)_3^{+2}$
			$^2Co(CO)_4^{+2}$	$^2Co(NH_3)_4^{+2}$	$^2Co(H_2O)_4^{+2}$
			$^2Co(CO)_5^{+2}$	$^2Co(NH_3)_5^{+2}$	$^2Co(H_2O)_5^{+2}$
			$^2Co(CO)_6^{+2}$	$^2Co(NH_3)_6^{+2}$	$^2Co(H_2O)_6^{+2}$
			M = Ni		
tier 1	$^1Ni_2$	$^1NiH_2$	$^1NiCH_2$	$^1NiN^+$	^3NiO
			$^1CH_3NiCO^+$	$^1NiN_2^{+2}$	^1HNiOH
tier 2			$^1Ni(CO)_1^{+2}$	$^1Ni(NH_3)_1^{+2}$	$^1Ni(H_2O)_1^{+2}$
			$^1Ni(CO)_2^{+2}$	$^1Ni(NH_3)_2^{+2}$	$^1Ni(H_2O)_2^{+2}$
			$^1Ni(CO)_3^{+2}$	$^1Ni(NH_3)_3^{+2}$	$^1Ni(H_2O)_3^{+2}$
			$^1Ni(CO)_4^{+2}$	$^1Ni(NH_3)_4^{+2}$	$^1Ni(H_2O)_4^{+2}$
			$^1Ni(CO)_5^{+2}$	$^1Ni(NH_3)_5^{+2}$	$^1Ni(H_2O)_5^{+2}$
			$^1Ni(CO)_6^{+2}$	$^1Ni(NH_3)_6^{+2}$	$^1Ni(H_2O)_6^{+2}$

[a] Tier 1 molecules are used to generate the diatomic repulsive potential curve, and tier 2 molecules are used to adjust the repulsive curve to reproduce B3LYP binding energies.

used at this stage of the parametrization to avoid additional complication; however, in certain cases, some open-shell molecules have also been included. Following the standard DFTB parametrization procedure, the thereby determined segments of the two-center repulsive potentials were connected to yield a continuous curve $E_{AB}^{\mathrm{rep}}(R)$ that was shifted up or down in energy so that the DFTB energetics of the larger test molecules (called tier 2) and also in some cases for some tier 3 molecules (see the next section for their definition) reasonably reproduces that of the DFT benchmark calculations at the B3LYP/SDD+6-31G(d) level (see the next section for definition of the basis set). Since $E_{AB}^{\mathrm{rep}}(R)$ has to be zero at R = ∞, the $E_{AB}^{\mathrm{rep}}(R)$ curve determined above was

Scheme 1. Schematic Representation of the Geometrical Parameters of the Set of Tier 3 Molecules for M = Ti, Fe, Co, and Ni[a]

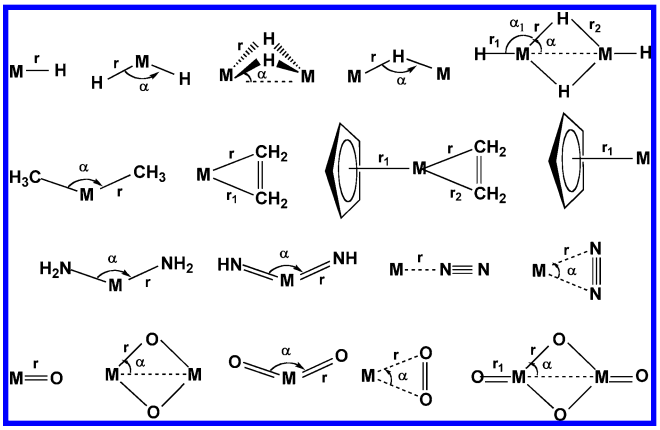

[a] For symmetric structures, only the unique parameters are given.

extrapolated smoothly to zero as R becomes large. The choice of various test molecules as well as the amount of the repulsion potential shift and the way of extrapolation are "empirical" procedures to determine the reliability of the DFTB parameters.

In the standard DFTB parametrization procedure all the two-center parameters, i.e., the overlap $S_{\mu\nu}$ and Hamiltonian $H_{\mu\nu}^0$ matrix elements between a set of valence orbitals μ and ν as well as the charge−charge interaction parameter γ_{AB} and the core−core repulsion E_{AB}^{rep} between the two atomic centers A and B are given in the tables as functions of interatomic distances.

Following the procedure outlined above, we have developed new spin-polarized DFTB parameters for transition-metal compounds containing Sc, Ti, Fe, Co, and Ni in combination with C, H, N, and O nonmetal elements as well as with themselves. These parameter tables have already been made available to the public free of charge at www.dftb.org.[25]

C. Tests of Determined Parameters. The newly developed parameter sets (used together with the DFTB parameters determined previously for the C, H, N, and O set) are tested against DFT results for a set of relatively small (called tier 3) molecules as well as larger, more realistic (tier 4) molecules. In the tier 3 set of molecules, we include strongly bonded small molecules as well as weakly bonded complexes. Some of these molecules are only hypothetical and are not known experimentally. In tier 4, larger compounds that are of greater interest for practical chemistry applications are chosen. Details concerning tier 4 molecules are given in each of the sections dealing with the individual metal atoms. Schematic structures of the molecule sets in tiers 3 and 4 are presented in Scheme 1 and Figures 1−4.

Benchmark DFT calculations are carried out with the B3LYP functional with a mixed basis set, Stuttgart/Dresden ab initio pseudopotential and (8s7p6d1f)/[6s5p3d1f] Gaussian valence basis set (SDD)[64,65] for transition-metal elements and the popular 6-31G(d) basis set for H, C, N, and O, unless otherwise noted. The mixed basis sets will be denoted as SDD+6-31G(d) in the remainder of this work. All DFT geometry optimizations have been performed using the Gaussian03[66] suite of programs, and the DFTB geometry

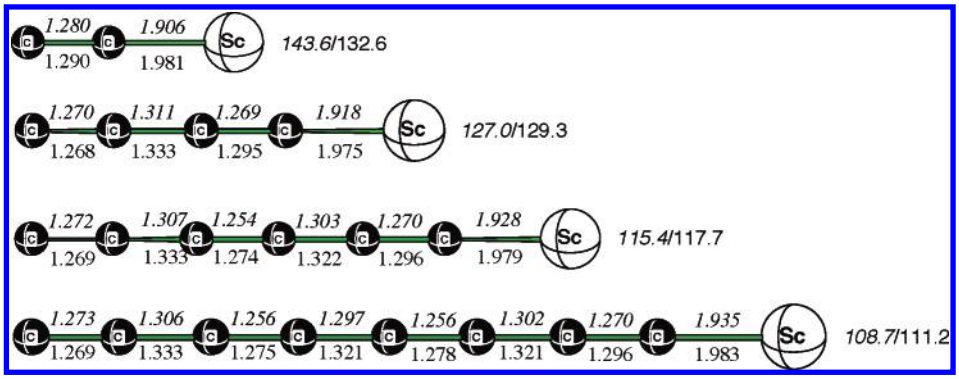

Figure 1. B3LYP/6-311+G(d) and SDFTB optimized bond distances (in Å) and Sc−C binding energies (in kcal/mol) for the electronic ^2S ground state of $Sc(CC)_n$ species, $n = 1-4$. Italic and plain values denote the DFT and SDFTB results, respectively.

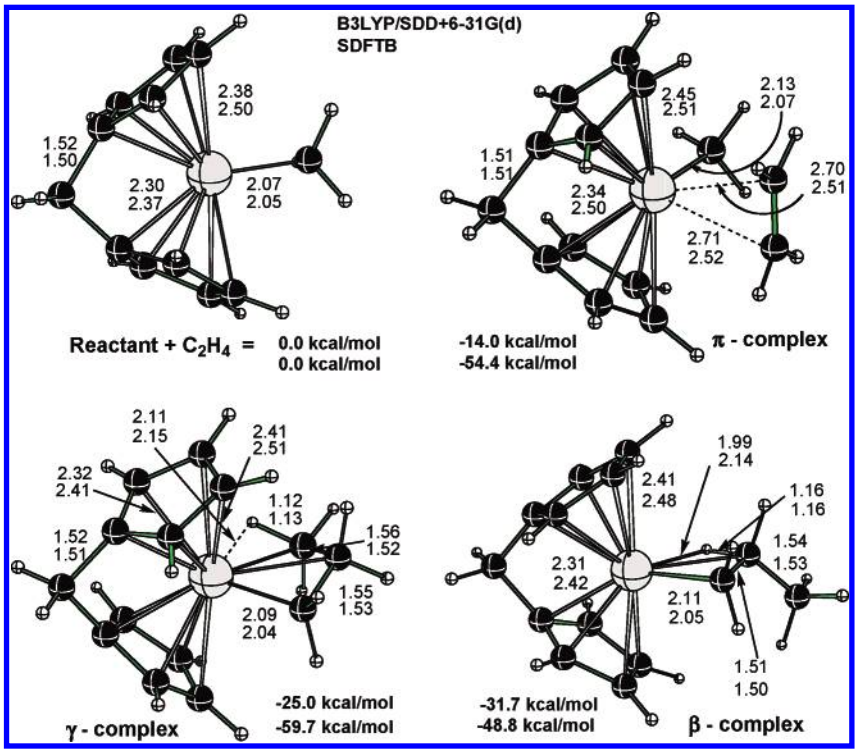

Figure 2. B3LYP/SDD+6-31G(d) (upper numbers) and SDFTB (lower numbers) optimized geometries (distances in Å) and energetics (in kcal/mol) of the reactant, intermediates, and product of the reaction $[(Cp\text{-}CH_2\text{-}Cp)TiCH_3]^+ + C_2H_4 \rightarrow [(Cp\text{-}CH_2\text{-}Cp)Ti(CH_2CH_2CH_3)]^+$.

optimizations were carried out using our own DFTB code.[38] Default values for gradient and displacement convergence criteria were applied throughout.

3. Results of Test Calculations

In this section we test the ability of DFTB using the presently developed parameters to reproduce common DFT (namely B3LYP/SDD+6-31G(d)) results, such as bond lengths, angles, and relative energetics. We emphasize that it is not the purpose of the present paper to discuss the ability of spin-polarized DFTB to reproduce experimental results but rather to investigate how far the approximations introduced in DFTB cause deviations from the benchmark DFT calculations. Therefore, available literature data on test molecules will not be discussed. We will only check the performance of DFTB based on the results compared with those at the B3LYP/SDD+6-31G(d) level (hereafter this level is simply called as DFT), unless otherwise noted. This was also the method used for evaluating the repulsive diatomic DFTB potentials. We compare the bond distances and angles for tier 3 molecules as well as the relative energies of low-lying spin states, since these are very important for transition-metal complexes. We did not compare simple bond dissociation energies such that $R_nM\text{-}XR'_m$, because often single-determinantal wave functions give incorrect spin states and make the direct energy comparison difficult.

A. Scandium. We present the geometrical parameters of Sc-containing tier 3 molecules in Table 3 for DFT and DFTB as well as the respective difference between the two levels of theory. We have dropped Sc_2O_x systems entirely as it was impossible to converge to proper wavefunctions and geometries. The absolute average bond distance difference for Sc−Sc is 0.17 Å (0.09 Å excluding very long distance in triplet $Sc_2(CH_3)_4$), Sc−H is 0.02 Å, for Sc−C 0.06 Å, for Sc−N

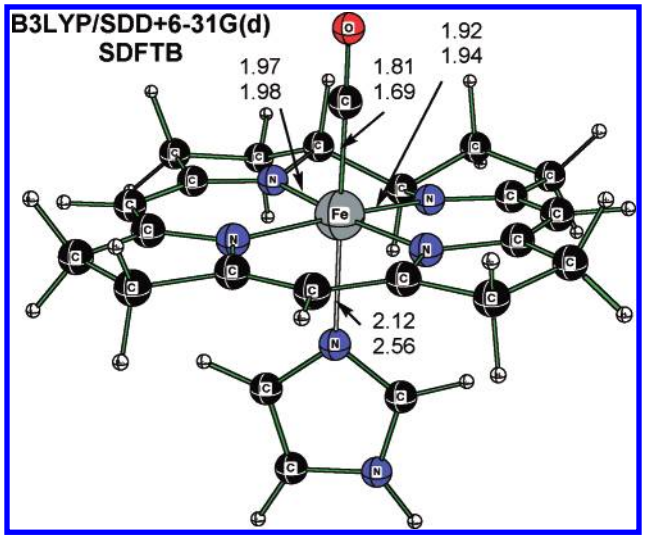

Figure 3. B3LYP/SDD+6-31G(d) (upper numbers) and SDFTB (lower numbers) optimized geometries (distances in Å) for the CO complex of Fe-porphyrin.

0.03 Å, and for Sc−O 0.03 Å. Sc−X bond lengths are therefore well described by the DFTB method with our parameters. Bond angle differences between DFT and DFTB results are on the absolute average 7.5° for Sc−Sc, 4.2° for Sc−H, 13.3° for Sc−C, 3.6° for Sc−N, and 28.4° for Sc−O. These deviations are generally much smaller than those we encountered for more d-electron rich transition-metal elements, further described below, indicating a better performance of the DFTB method when fewer d-electrons are present. The large discrepancy for the O−Sc−O bond in the quartet state of the ScO_2 molecule with 43.7° is an exception; because of the lack of more angle parameters, the average absolute value of Sc−O angle deviations is large. The overall average absolute bond distance difference between DFTB and DFT is 0.04 Å, and the overall average absolute bond angle difference is 12.4°. Therefore, generally speaking, DFTB geometries are in reasonable agreement with those predicted by DFT.

In Table 4 the dissociation energies of Sc-containing molecules are shown. The results are scattered, with some very good values and some poor values. Sc−H bridge bonds are overbound in DFTB, while Sc−N bonds are underbonds. A large error in the ScO_2 (2) → Sc (2) + O_2 (3) proves it is due to the fact SDFTB is unable to describe the triplet state of O_2 correctly.

In Table 5 the relative energies of high-spin and low-spin states of Sc-containing molecules are shown. The DFT energy orders are reproduced by DFTB except for Sc_2H and $Sc^+(\eta^2\text{-}N_2)$, where state splittings are relatively small. Although the magnitude of state splitting difference between DFT and DFTB can be as large as 38 kcal/mol (in the case of Sc_2H), the average absolute differences between DFT and DFTB state splitting energies are 13.1 kcal/mol for Sc−Sc, 14.2 kcal/mol for Sc−H, 14.0 kcal/mol for Sc−C, 18.1 kcal/mol for Sc−N, and 15.4 kcal/mol for Sc−O compounds. This performance is better than for d-electron rich transition-metal elements, as we already noted for geometries. The overall average deviation is 15.1 kcal/mol. We report an overall tendency in DFTB to overestimate the binding energies of low-spin complexes. Consequently, DFTB energetics should be carefully checked in the case of scandium parameters but are more reliable in general than for d-electron rich elements (see below).

As an example of a tier 4 molecule, in Figure 1, we compare B3LYP/6-311+G(d) geometries and energies of linear $Sc(CC)_n$ (n=1, 2, 3, 4) in their electronic ^2S ground states with the corresponding DFTB results. The DFT results were already partially presented by Redondo et al.[28] who however did not provide the Sc−C binding energies for this series of polyyne chains. As one can see, DFTB structural results are in reasonable agreement with the B3LYP calculations, with bond differences the largest for the Sc−C bond. Here, DFTB gives bond lengths that are too long by up to 0.08 Å. As for the C−C bond lengths, the DFTB values are consistently longer compared to the B3LYP/6-311+G(d) results for both short/long alternating bond types. Energetics is in excellent agreement, with DFTB overbinding by only 3 kcal/mol, except for the special case of ScC_2 where DFTB underbinds by about 10 kcal/mol in this most strongly bound species due to the overstabilization of the C_2 unit.

B. Titanium. As shown in Table 6, the present set of Ti DFTB spin-polarized parameters leads to optimized geometries close to those obtained by DFT. The average absolute deviations between bond lengths obtained by DFT and DFTB are 0.05 Å for Ti−H, 0.06 Å for Ti−C, 0.02 Å for Ti−N, and 0.03 Å for Ti−O, respectively. Also, bond angles are reasonably described by DFTB when compared with those obtained by DFT, with the average deviation of angles for all tier 3 molecules studied here being 7.0°. However, individual angular deviations can be quite large, for instance the deviation of the DFTB Ti−H−Ti angle from the DFT angle in Ti_2H is 37.4°, leading to a too strongly bent DFTB structure in this case. Other Ti−H−Ti angles are described much better, and their deviations range from 0° to about 15°, following no obvious trend of either too sharp or too flat angles. The same holds true for Ti−X−Ti and X−Ti−X angles with X = C, N, and O, with the only exception of $Ti(O_2)$. In this T-shaped molecule, the main failure lies in the underestimated Ti−O bond distance in DFTB, leading to a too sharp O−Ti−O angle. Problems of DFTB with the Ti−O parameter sets obviously are encountered for such polar Ti π-complexes, which is not surprising considering the fact that tiers 1 and 2 molecule sets did not include such weak bonding situations. Overall, the performance of our Ti parameters for DFTB optimized geometries is very reasonable, especially given the fact that the change of basis sets and density functionals can result in similar deviations among DFT calculations. Therefore, we conclude that the geometry performance of DFTB is acceptable for the Ti−X systems.

In Table 7 the dissociation energies of Ti-containing compounds are shown. All the bonds seem to be substantially overbound with the DFTB methods.

Relative energies (relative to the respective high-spin states) of the lower-lying electronic states of tier 3 Ti-containing molecules for DFT and DFTB as well as the absolute deviation between relative energies for the two respective methods are given in Table 8. The relative energy

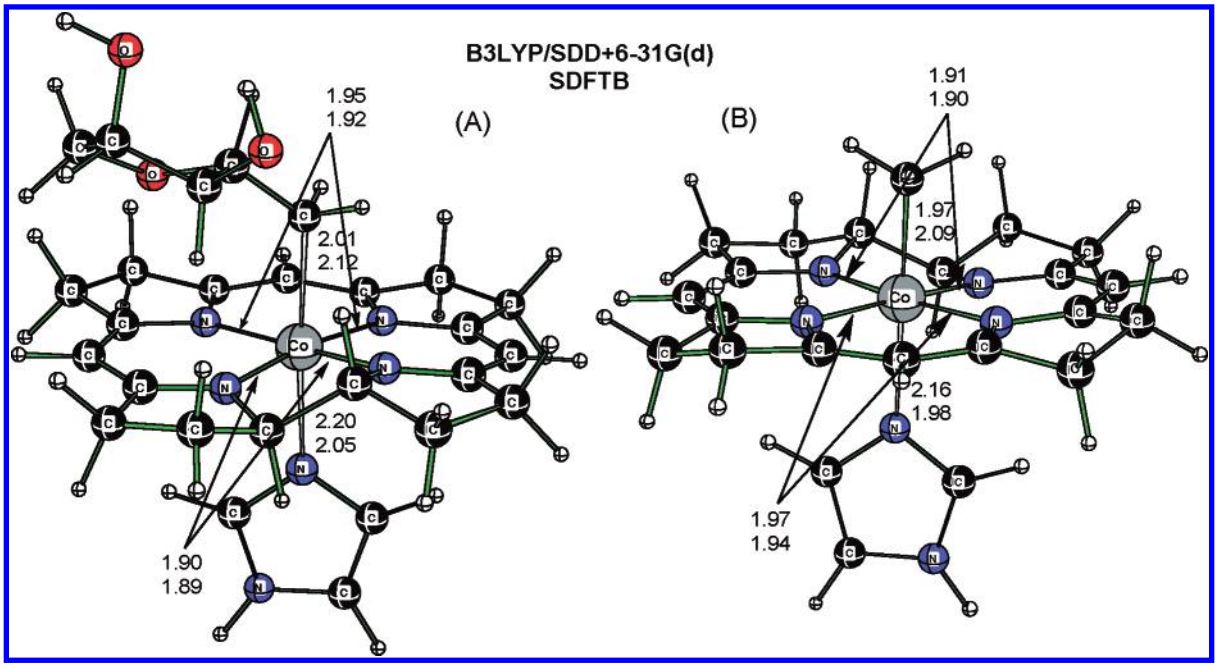

Figure 4. B3LYP/SDD+6-31G(d) (upper numbers) and SDFTB (lower numbers) optimized geometries (distances in Å) geometries of adenosylcobalamin and methylcobalamin.

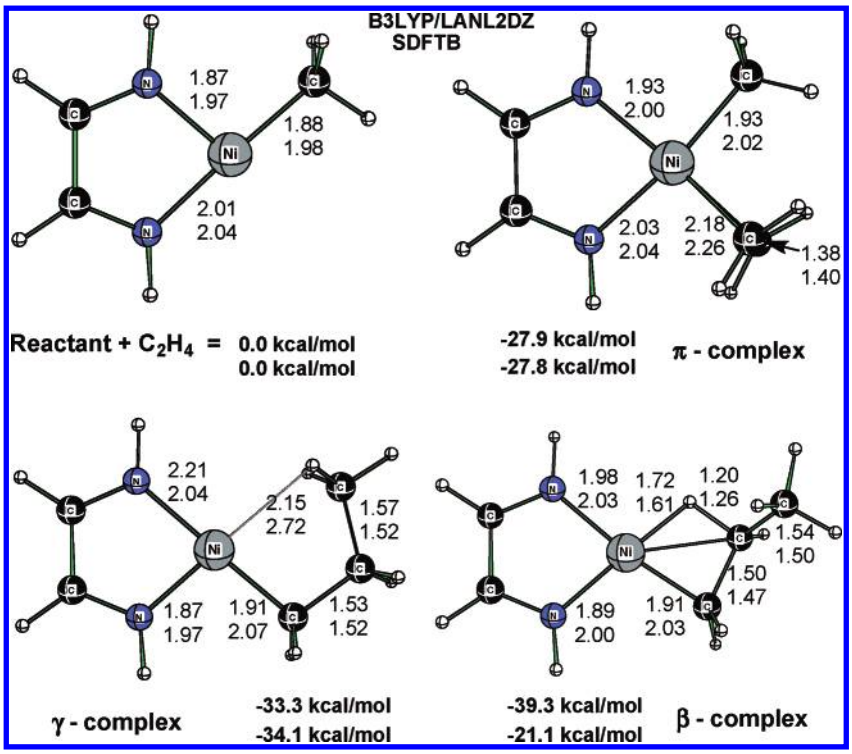

Figure 5. B3LYP/Lanl2DZ (upper numbers) and SDFTB (lower numbers) optimized geometries (distances in Å) and energetics (in kcal/mol) of the reactant, intermediates, and product of the ethylene insertion step of ethylene polymerization: $[(NHCHCHNH)NiCH_3]^+ + CH_2{=}CH_2 \rightarrow [(NHCHCHNH)NiCH_2CH_2CH_3]^+$.

order between high- and low-spin states predicted by DFT is reproduced by DFTB in most cases. However, the difference between DFTB and DFT relative energies can be as large as 25 kcal/mol, as was encountered for the TiO molecule where the low-spin state is appreciably overstabilized in the DFTB method. Partially this difference can be explained by the well-known fact that B3LYP shows a preference for the high-spin state due to the inclusion of exact Hartree−Fock exchange, whereas spin-dependent atomic parameters in DFTB are derived from the nonhybrid PBE density functional. A similar tendency for low-spin state stabilization is also seen in the case of the molecules Ti_2H_2, Ti_2H, and $Ti(C_2H_4)^+$, where the B3LYP high-spin states are actually lower in energy than the respective low-spin states, while DFTB predicts a reverse energetic ordering. However, these molecules feature relatively small spin state splittings in DFT (smaller than 10 kcal/mol), and the sign change in DFTB is therefore within the average absolute deviation of

Table 3. DFTB and DFT (B3LYP/SDD+6-31G(d)) Optimized Bond Lengths (Å) and Valence Angles (°) of Sc-Containing Tier 3 Molecules, for the Geometry Parameters Defined in Scheme 1

compound	multiplicity	parameter	DFT	SDFTB	Δ(DFTB−DFT)
		Sc−Sc			
$Sc_2(CH_3)_2$	1	r	2.79	2.75	−0.04
		r_1	2.17	2.18	0.01
		α	109.8	103.1	−6.7
	3	r	2.57	2.76	0.19
		r_1	2.18	2.18	0.00
		α	180.0	180.0	0.0
$Sc_2(CH_3)_4$	1	r	2.81	2.78	−0.03
		r_1	2.16	2.17	0.01
		α	115.7	106.3	−9.4
	3	r	3.19	2.77	−0.42
		r_1	2.18	2.19	0.01
		α	121.6	107.9	−13.7
		Sc−H			
ScH	1	r	1.74	1.77	0.03
	3	r	1.84	1.83	−0.01
ScH_2	2	r	1.81	1.81	0.00
		α	118.5	123.6	−5.1
	4	r	1.96	1.90	0.06
		α	180.0	180.0	0.0
Sc_2H_2	1	r	1.96	1.99	0.03
		α	75.4	72.7	−2.7
	3	r	1.97	1.98	0.01
		α	74.1	84.5	−10.4
Sc_2H	2	r	1.95	1.98	0.03
		α	73.2	73.8	0.6
	4	r	1.93	1.99	0.06
		α	84.4	87.0	2.6
Sc_2H_4	1	r	1.97	1.99	0.02
		r_1	1.84	1.83	−0.01
		r_2	1.97	1.99	0.02
		α	48.7	46.5	−2.2
		α_1	137.7	128.0	−9.7
		Sc−C			
$Sc(CH_3)_2^+$	1	r	2.09	2.08	−0.01
		α	104.2	105.1	0.9
	3	r	2.33	2.21	−0.12
		α	113.1	138.8	25.7
$Sc(C_2H_4)^+$	1	r	2.07	2.08	0.01
	3	r	2.36	2.27	−0.11
		r_1	2.36	2.27	−0.11
$CpSc(C_2H_4)^+$	2	r	2.40	2.30	−0.10
		r_1	2.40	2.35	−0.05
$ScCp^+$	2	r_1	2.35	2.30	−0.05
	4	r_1	2.35	2.30	−0.05
		Sc−N			
$Sc(NH_2)_2^+$	1	r	1.88	1.81	−0.07
		α	176.5	180.0	3.5
	3	r	1.83	1.85	0.02
		α	180.0	180.0	0.0
$Sc(NH)_2$	2	r	1.84	1.86	0.02
		α	104.9	115.8	10.9
	4	r	1.96	1.95	−0.01
		α	180.0	180.0	0.0
$Sc^+(\eta^1\text{-}N_2)$	1	r	2.06	2.02	−0.04
	3	r	2.09	2.04	−0.05
$Sc^+(\eta^2\text{-}N_2)$	1	r	2.03	2.04	0.01

Table 3. (Continued)

compound	multiplicity	parameter	DFT	SDFTB	Δ(DFTB−DFT)Sc−O
	3	r	2.17	2.14	−0.03
ScO	2	r	1.66	1.67	0.01
	4	r	1.86	1.92	0.06
ScO_2	2	r	1.77	1.78	0.01
		α	127.1	114.1	−13.0
	4	r	1.92	1.89	−0.03
		α	122.9	79.2	−43.7
$Sc(O_2)$	2	r	1.85	1.90	0.05
	4	r	2.11	2.08	−0.03

Table 4. SDFTB and DFT (B3LYP/SDD+6-31G(d)) Dissociation Energies of Tier 3 Sc-Containing Molecules

	dissociation energy (kcal/mol)		
dissociation process[a]	DFT	DFTB	Δ(DFTB−DFT)
Sc−H			
Sc_2H_2 (1) → 2 ScH (1)	41.3	64.6	23.3
Sc_2H_4 (1) → 2 ScH_2 (2)	48.4	68.2	19.8
Sc−C			
$Sc(CH_3)_2^+$ (1) → Sc^+ (3) + C_2H_6	34.6	36.7	2.2
$Sc(C_2H_4)^+$ (1) → Sc^+ (3) + C_2H_4	35.0	36.4	1.4
Sc−N			
$Sc(NH_2)_2^+$ (1) → Sc^+ (3) + N_2H_4	137.1	142.7	5.6
$Sc(NH)_2$ (2) → Sc (2) + N_2H_2	180.4	136.5	−43.9
$Sc^+(N_2)$ (1) → Sc^+ (3) + N_2	9.4	12.5	3.1
Sc−O			
ScO_2 (2) → Sc (2) + O_2 (3)	129.0	176.0	47.1

[a] The numbers in parentheses represent the spin multiplicity.

Table 5. SDFTB and DFT (B3LYP/SDD+6-31G(d)) Energies (Relative to the Respective High-Spin States) of the Low-Lying Electronic States of Tier 3 Sc-Containing Molecules

		relative energies (kcal/mol)		
compound	multiplicities[a]	DFT	SDFTB	Δ(DFTB−DFT)
		Sc−Sc		
$Sc_2(CH_3)_2$	3 → 1	7.2	−13.0	−20.3
$Sc_2(CH_3)_4$	3 → 1	−9.5	−15.3	−5.8
		Sc−H		
ScH	3 → 1	−4.3	−2.1	2.2
ScH_2	4 → 2	−87.6	−63.0	24.7
Sc_2H_2	3 → 1	6.7	0.3	−6.4
Sc_2H	4 → 2	8.8	−29.4	−38.2
Sc_2H_4	3 → 1	−3.8	−5.4	−1.6
		Sc−C		
$Sc(CH_3)_2^+$	3 → 1	−51.4	−62.4	−10.9
$Sc(C_2H_4)^+$	3 → 1	−1.4	−24.0	−22.6
$ScCp^+$	4 → 2	−74.1	−65.6	8.5
		Sc−N		
$Sc(NH_2)_2^+$	3 → 1	−49.2	−71.2	−22.1
$Sc(NH)_2$	4 → 2	−45.7	−71.5	−25.8
$Sc^+(\eta^1\text{-}N_2)$	3 → 1	21.5	11.6	−10.0
$Sc^+(\eta^2\text{-}N_2)$	3 → 1	5.9	−8.7	−14.6
		Sc−O		
ScO	4 → 2	−76.8	−94.5	−17.7
ScO_2	4 → 2	−58.5	−86.2	−27.7
$Sc(O_2)$	4 → 2	−43.9	−44.7	−0.8

[a] For instance, 3 → 1 means that the energy of the singlet (low-spin) state relative to the triplet (high-spin) state.

13.7 kcal/mol. Therefore we conclude that DFTB predicts the relative energy order between high- and low-spin states in most cases reasonably well.

As to a tier 4 system, we tested one specific reaction $[(Cp\text{-}CH_2\text{-}Cp)TiCH_3]^+ + C_2H_4 \rightarrow [(Cp\text{-}CH_2\text{-}Cp)Ti(CH_2CH_2\text{-}CH_3)]^+$ exemplifying a polymerization processes involving a Ti catalyst. DFT and DFTB geometries as well as respective energetics are presented in Figure 2. In this "real-life" scenario, again we find that the DFT geometries of Ti-containing species are reasonably well reproduced by DFTB with bond length differences of at most about 0.1 Å. However, the relative stability of these complexes as predicted by DFT is not reproduced by DFTB, which shows a strong tendency to overbinding of ethylene and results in smearing out subtle energetic differences of a few kcal/mol between isomeric complexes that are predicted by DFT. This finding shows that DFTB binding energies are not as reliable as geometrical parameters and have to be used with great caution.

C. Iron. In Table 9, the geometries of tier 3 molecules optimized at DFT and DFTB levels are listed. The average absolute deviation of DFTB results from DFT is 0.09 Å for Fe−H, 0.08 Å for Fe−C, 0.10 Å for Fe−N, and 0.06 Å for Fe−O bond distances. These values are again within 0.1 Å, which we consider to be acceptable, considering comparable geometrical changes introduced by the change of basis set and/or density functional for DFT calculations. Bond angles perform better for X−Fe−X and Fe−X−Fe than for the corresponding Ti systems, with average absolute deviations of 9.6° for Fe−H, 6.5° for Fe−C, 12.9° for Fe−N, and 11.2° for Fe−O systems. The largest deviations in bond angles are actually found for $Fe(NH_2)_2$ and FeO_2 systems with about 30°. For these compounds, qualitatively different geometries are predicted by DFTB when compared to DFT (bent structure vs linear or vice versa). This difference may stem from the fact that in DFTB parametrization the d^7s^1 configuration is used, which prefers a linear structure arising from sd hybridization. Concerning the overall performance of DFTB for geometrical parameters however, we find that bond distances and angles of DFT geometries are typically well reproduced by DFTB.

In Table 10 the dissociation energies of Fe-containing compounds are given. Bridged Fe−H bonds are underbound while the terminal Fe−H bonds are overbound, while Fe−C

Table 6. SDFTB and DFT (B3LYP/SDD+6-31G(d)) Optimized Bond Lengths (Å) and Valence Angles (°) of Ti-Containing Tier 3 Molecules, for the Geometry Parameters Defined in Scheme 1

compound	multiplicity	parameter	DFT	SDFTB	Δ(DFTB−DFT)
		Ti−H			
TiH	2	r	1.68	1.74	0.06
	4	r	1.84	1.76	−0.08
TiH_2	1	r	1.75	1.71	−0.04
		α	106.9	111.9	5.0
	3	r	1.78	1.74	−0.04
		α	122.3	108.3	−14.0
Ti_2H	2	r	1.86	1.89	0.03
		α	102.0	64.6	−37.4
	4	r	1.82	1.93	0.11
		α	83.0	75.1	−7.9
Ti_2H_2	1	r	1.86	1.80	−0.06
		α	48.3	57.8	9.5
	3	r	1.87	1.88	0.01
		α	57.2	57.3	0.1
Ti_2H_4	1	r	1.85	1.87	0.02
		r_1	1.74	1.75	0.01
		α	58.0	55.2	−2.8
		Ti−C			
$Ti(CH_3)_2$	1	r	2.04	2.05	0.01
		α	110.7	112.5	1.8
	3	r	2.18	2.08	−0.10
		α	117.1	114.8	−2.3
$Ti(C_2H_4)^+$	2	r	2.03	2.00	−0.03
	4	r	2.34	2.26	−0.08
$TiCp^+$	1	r_1	2.26	2.20	−0.06
	3	r_1	2.27	2.27	0.00
		Ti−N			
$Ti(NH_2)_2^+$	2	r	1.85	1.84	−0.01
		α	118.3	115.1	−3.2
$Ti(NH)_2$	1	r	1.71	1.70	−0.01
		α	114.8	117.7	3.1
$Ti^+(\eta^1\text{-}N_2)$	2	r	1.99	2.00	0.01
		Ti−O			
TiO	1	r	1.59	1.59	0.00
	3	r	1.61	1.61	0.00
Ti_2O_2	1	r	1.81	1.91	0.10
		α	51.4	52.0	0.6
TiO_2	1	r	1.64	1.64	0.00
		α	117.7	111.5	−6.2
$Ti(O_2)$	1	r	1.79	1.81	0.02
		α	49.3	56.4	7.1
Ti_2O_4	1	r	1.84	1.84	0.00
		r_1	1.63	1.63	0.00
		α	42.6	47.7	5.1

are acceptable. Both terminal and bridged FeO bonds seem to be grossly overbound.

The relative energies between different spin states of the Fe-containing tier 3 molecules are shown in Table 11. DFTB predicts usually the same energetic order as the one computed by DFT. Fe_2H, FeO, FeO_2, $Fe(O_2)$, and Fe_2O_4 molecules are an exception to this rule with a reversed energy order of low- and high-spin states. Similarly to Ti, B3LYP generally favors high-spin states when compared with the DFTB approach. This is however not true for all cases; for instance, the quartet state of $Fe(\eta^2\text{-}N_2)$ is 38.3 kcal/mol lower in energy relative to the doublet state in DFTB than in DFT. In general, relative energy differences between high-spin state and low-spin state between DFT and DFTB can be as large as 40 kcal/mol.

Table 7. SDFTB and DFT (B3LYP/SDD+6-31G(d)) Dissociation Energies of Tier 3 Ti-Containing Molecules

dissociation process	dissociation energy (kcal/mol) DFT	DFTB	Δ(DFTB−DFT)
Ti−H			
Ti_2H_2 (3) → 2 TiH (4)	73.2	106.9	33.7
Ti_2H_4 (1) → 2 TiH_2 (3)	44.1	111.8	67.7
Ti−C			
$Ti(C_2H_4)^+$ (4) → Ti^+ (2) + C_2H_4	75.6	88.9	13.3
$CpTi(C_2H_4)$ (2) → TiCp (4) + C_2H_4	35.9	63.1	27.2
Ti−N			
$Ti(NH)_2$ (1) → Ti (3) + N_2H_2	98.8	137.0	38.2

Table 8. SDFTB and DFT (B3LYP/SDD+6-31G(d)) Energies (Relative to the Respective High-Spin States) of the Low-Lying Electronic States of Tier 3 Ti-Containing Molecules

compound	multiplicities[a]	relative energies (kcal/mol) DFT	SDFTB	Δ(DFTB−DFT)
		Ti−H		
TiH	4 → 2	1.2	19.7	18.5
TiH_2	3 → 1	39.8	14.2	−25.6
Ti_2H_2	3 → 1	2.1	−10.0	−12.1
Ti_2H_4	3 → 1	24.9	45.8	20.9
		Ti−C		
$Ti(CH_3)_2$	3 → 1	5.9	12.7	6.8
$Ti(C_2H_4)^+$	4 → 2	8.2	−3.6	−11.8
$TiCp^+$	3 → 1	12.0	13.6	1.6
		Ti−O		
TiO	3 → 1	31.4	6.4	−25.0

[a] For instance, 3 → 1 means that the energy of the singlet (low-spin) state relative to the triplet (high-spin) state.

As a tier 4 molecule, binding of CO to a heme molecule with an axial histidine residue has been investigated. The structure of this complex is shown in Figure 3. The DFT geometry is well reproduced by DFTB. The only exceptions are the $Fe-N_{imidazole}$ and Fe−C distance trans to $Fe-N_{imidazole}$, which are 0.44 Å too long and 0.12 Å too short, respectively, in DFTB. The computed binding energy of CO is 55.7 kcal/mol for DFT, while for DFTB it is only 26.5 kcal/mol despite the short Fe−CO distance. This is in contrast to the case of π and σ bonding of ethylene to a Ti complex discussed above, where DFTB predicts generally too large binding energies. Again, DFTB energetics may have to be used with great caution.

D. Cobalt. The structural parameters of Co-containing tier 3 molecules for both DFT as well as DFTB, and the respective relative differences are listed in Table 12. As observed for the cases of Sc, Ti, and Fe, the Co DFTB

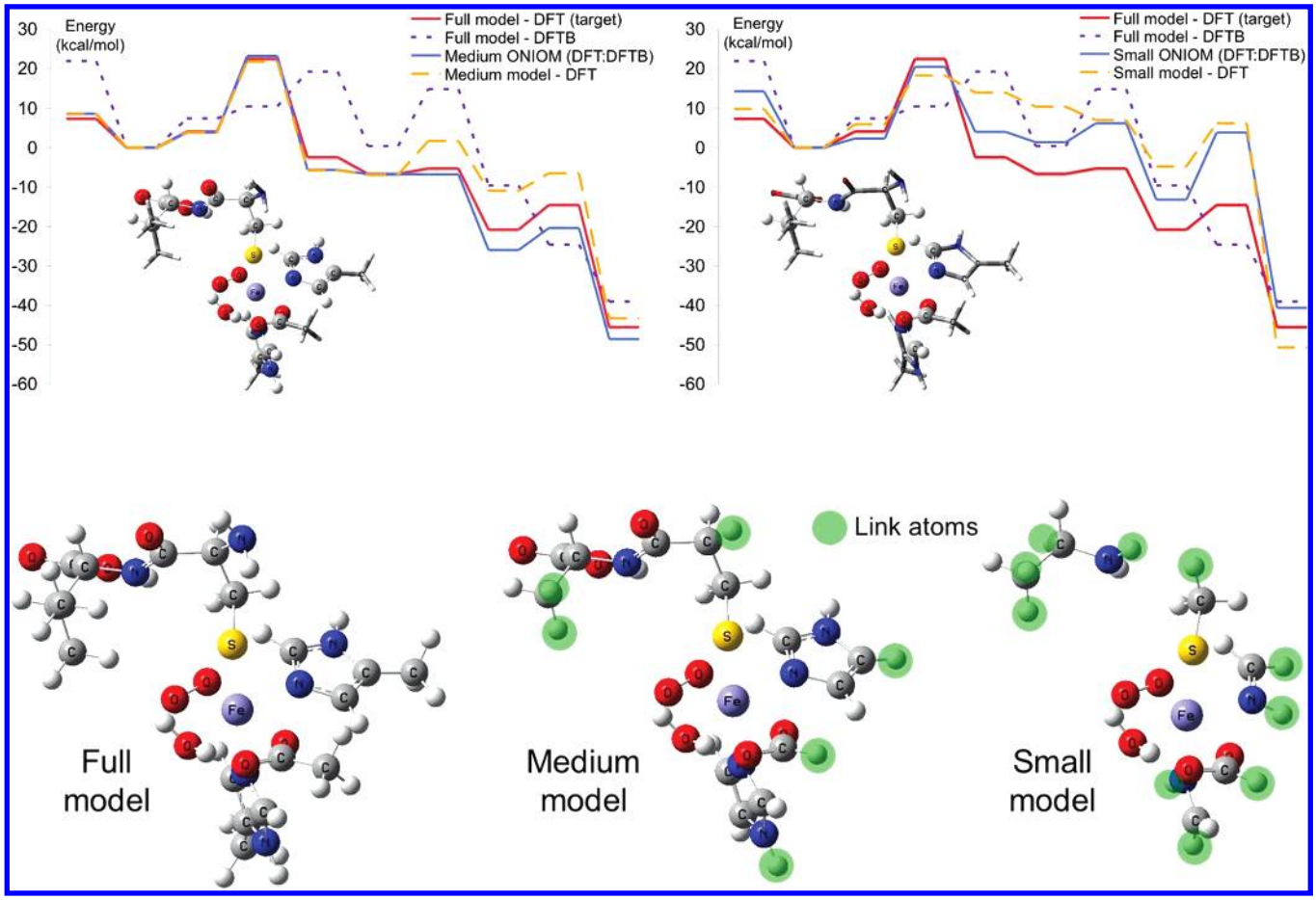

Figure 6. Stationary points along the reaction coordinate for a redox reaction involving iron. The red line represents B3LYP/6-31G(d) energies, the blue line represents DFTB energies, while the purple line shows the results from ONIOM (DFT:DFTB). Energies are aligned at the second stationary point. DFT and DFTB-only calculations include all atoms in the model. For the ONIOM system, the high-level part of is shown in ball-and-stick representation, while the DFTB part is shown in licorice representation.

geometries are in good agreement with DFT optimized structures. Compared with DFT results, the average absolute deviation of bond distance is 0.04 Å for Co−H, 0.06 Å for Co−C, 0.03 Å for Co−N, and 0.01 Å for Co−O. For bond angles, the average absolute deviation of DFTB from DFT is 5.0° for Co−H, 5.7° for Co−C, 9.9° for Co−N, and 6.9° for Co−O parameters. Some linear structures are preferred in DFTB results presumably due to d^8s^1 Co atomic configuration used in parametrization, a phenomenon described above for Fe. Yet, X−Co−X and Co−X−Co angles are generally in better agreement with DFT structural parameters than for corresponding Fe and Ti systems. We cannot comment at this stage on the origin of this exceptional good performance of Co DFTB parameters. Overall, from the average deviation values discussed above, we conclude that DFTB very reasonably reproduces DFT geometries in the case of Co-containing compounds.

The dissociation energies of Co-containing compounds are shown in Table 13. Co−H bonds are overbounds, while Co−C, C, and O bonds are all overbound.

The relative energy order between high-spin and low-spin states for different Co containing molecules are summarized in Table 14. The relative energy orders in DFT are well reproduced by DFTB except CoH_2, $Co(CH_3)_2$, $CpCo(C_2H_4)^+$, $CoCp^+$, and $Co(NH_2)_2$. Considering their high-spin states are favored by B3LYP, DFTB reasonably predict the relative energy order although the absolute values deviation is 20.7 kcal/mol on the average, with the largest difference being about 54 kcal/mol in the case of $CoCp^+$. Particularly noticeable is the DFTB preference for low-spin states in the case of Co−C systems, but noticeable exceptions from this rule exist, for instance Co_2H_4, where DFTB favors the high-spin state by 21 kcal/mol relative to DFT.

As a real case tier 4 system, binding of adenosyl and methyl groups, respectively, to cobalamin has been investigated. The molecular structures of adenosylcobalamin and methylcobalamin are shown in Figure 4. The geometries in both structures are well described by DFTB compared with the corresponding structures from DFT. The largest bond distance difference is about 0.18 Å in only one case. Again, DFTB predicts Co−N bond distance orders correctly. The binding energy of the adenosyl group to cobalamin is 70.3 kcal/mol in DFTB, that is 12.5 kcal/mol higher in comparison to 57.8 kcal/mol in DFT. Similarly, the binding energy of the methyl group to cobalamin is 94.3 kcal/mol in DFTB, that is an overbinding of 22.2 kcal/mol when compared to 72.1 kcal/mol in DFT. Thus, it is concluded that DFTB performs well in terms of geometries. Again we should

Table 9. SDFTB and DFT (B3LYP/SDD+6-31G(d)) Optimized Bond Lengths (Å) and Valence Angles (°) of Fe-Containing Tier 3 Molecules, for the Geometry Parameters Defined in Scheme 1

compound	multiplicity	parameter	DFT	SDFTB	Δ(DFTB−DFT)
		Fe−H			
FeH	2	r	1.59	1.50	−0.09
	4	r	1.56	1.54	−0.02
FeH_2	3	r	1.54	1.51	−0.03
		α	102.4	96.9	−5.5
	5	r	1.65	1.62	−0.03
		α	169.7	153.0	−16.7
Fe_2H	2	r	1.68	1.66	0.02
		α	46.45	50.79	4.34
Fe_2H_4	1	r	1.52	1.52	0.00
		r_1	1.65	1.49	0.16
		α	46.79	63.9	17.11
Fe_2H_4	3	r	1.58	1.60	0.02
		r_1	1.61	1.72	0.11
		α	47.27	48.87	1.60
		Fe−C			
$Fe(CH_3)_2$	1	r	1.92	2.06	0.14
		α	117.7	112.2	−5.5
	3	r	1.94	2.07	0.13
		α	112.1	109.3	−2.8
	5	r	2.05	2.13	0.08
		α	180.0	180.0	0.0
$Fe(C_2H_4)^+$	2	r	2.05	2.13	0.08
	4	r	2.07	2.18	0.11
$FeCp^+$	3	r_1	2.19	2.26	0.07
	5	r_1	2.23	2.32	0.09
		Fe−N			
$Fe(NH_2)_2$	1	r	1.79	1.76	0.03
		α	180.0	150.7	−29.3
	5	r	1.85	1.86	0.01
		α	180.0	180.0	0.0
$Fe(NH)_2$	3	r	1.65	1.60	−0.05
		α	171.2	180.0	8.8
	5	r	1.67	1.76	0.09
		α	121.1	142.1	21.0
$Fe(\eta^1\text{-}N_2)^+$	4	r	2.09	1.92	−0.17
		α	0.00	0.01	0.01
		Fe−O			
FeO	1	r	1.59	1.58	−0.01
	3	r	1.57	1.61	0.04
	5	r	1.61	1.66	0.05
Fe_2O_2	1	r	1.73	1.80	0.07
		α	42.8	51.8	9.0
	3	r	1.76	1.81	0.05
		α	42.8	52.6	9.8
FeO_2	1	r	1.54	1.61	0.07
		α	145.2	167.6	22.4
	3	r	1.58	1.63	0.05
		α	140.4	149.4	9.0
	5	r	1.60	1.67	0.07
		α	118.7	126.0	7.3
$Fe(O_2)^+$	4	r	1.82	1.81	−0.01
		α	43.8	44.1	0.3
Fe_2O_4	1	r_1	1.56	1.57	0.01
		r	1.72	1.81	0.09
		α	47.6	44.4	−3.2
	3	r_1	1.53	1.59	0.06
		r	1.74	1.80	0.06
		α	43.9	45.4	1.5

Table 10. SDFTB and DFT (B3LYP/SDD+6-31G(d)) Dissociation Energies of Tier 3 Fe-Containing Molecules

	dissociation energy (kcal/mol)		
dissociation process	DFT	DFTB	Δ(DFTB−DFT)
	Fe−H		
Fe_2H_4 (1) → 2FeH_2 (3)	79.7	54.5	−25.2
FeH_2 (1) → Fe (1) + H_2 (1)	86.9	105.2	18.3
FeH_2 (1) → FeH (2) + H	61.9	90.6	28.7
	Fe−C		
$Fe(CH_3)_2$ (2) → Fe (2) + C_2H_6	21.3	34.9	13.6
$Fe(C_2H_4)$ (2) → Fe (2) + C_2H_4	56.3	52.5	−3.8
	Fe−O		
Fe_2O_2 (1) → 2FeO (1)	84.6	133.8	49.2
Fe_2O_4 (1) → 2FeO_2 (1)	68.9	119.2	50.3

caution about the use of DFTB for the prediction of energetics due to the unforeseeable over- or underbinding errors.

E. Nickel. The geometrical parameters of Ni-containing tier 3 molecules are shown in Table 15 for DFT and DFTB as well as the respective difference between the two levels of theory. In the case of triplet $Ni_2(CH_3)_4$, DFT predicts an asymmetric structure with one bridging methyl group, whereas the DFTB triplet geometry resembles more closely the symmetric DFTB singlet geometry. The average absolute bond distance difference is 0.15 Å for Ni−Ni, 0.06 Å for Ni−H, 0.19 Å for Ni−C, 0.04 Å for Ni−N, and 0.02 Å for Ni−O. The Ni−C distance is not well described in cases where cyclopentadienyl (Cp) rings interact with Ni. Here, Ni−C bonds are typically too long by a few tenths of an angstrom, mainly because the position of the Ni on top of the Cp system is very flexible. Bond angle differences between DFT and DFTB results are on the absolute average 16.2° for Ni−Ni, 12.2° for Ni−H, 18.8° for Ni−C, 30.8° for Ni−N, and 7.7° for Ni−O. The rather large deviations are a consequence of the fact that DFTB very often prefers linear arrangements, when the lowest DFT structure is bent (as seen also for Fe and Co above). The overall average absolute bond distance difference between DFTB and DFT is 0.09 Å, and the overall average bond angle difference is 17.1°. Therefore, more generally speaking, DFTB geometries are in reasonable agreement with those predicted by DFT, which is consistent with the findings in the case of other transition-metal elements in this work.

The dissociation energies of Ni-containing compounds are shown in Table 16. Most of the Ni bonds seem to be underbound substantially.

In Table 17, the relative energies of high-spin and low-spin states of Ni-containing molecules are shown. The DFT energy orders are reproduced by DFTB except for Ni_2H_2, $NiCp^+$, $Ni(NH_2)_2^+$, NiO_2, and $Ni(O_2)$, where state splittings are generally very small. However, the magnitude of state splitting difference between DFT and DFTB can be as large as 50 kcal/mol (in the case of Ni_2H_4). Average absolute differences between DFT and DFTB state splitting energies are 32.4 kcal/mol for Ni−H, 14.9 kcal/mol for Ni−C, 19.8 kcal/mol for Ni−N, and 20.6 kcal/mol for Ni−O. The overall average absolute deviation is 21.9 kcal/mol. Again we report

Table 11. SDFTB and DFT (B3LYP/SDD+6-31G(d)) Energies (Relative to the Respective High-Spin States) of the Low-Lying Electronic States of Tier 3 Fe-Containing Molecules

		relative energies (kcal/mol)		
compound	multiplicities[a]	DFT	SDFTB	Δ(DFTB−DFT)
		Fe−H		
FeH	4 → 2	43.7	33.5	−10.2
FeH_2	3 → 1	22.0	11.7	−10.3
		Fe−C		
$Fe(CH_3)_2$	3 → 1	33.1	19.7	−13.4
$Fe(C_2H_4)^+$	4 → 2	41.6	32.4	−9.2
$FeCp^+$	5 → 3	13.8	16.7	2.9
		Fe−N		
$Fe(NH_2)_2$	5 → 1	33.3	12.4	−20.9
$Fe(NH)_2$	5 → 3	8.2	27.6	19.4
Fe(η^1-N_2)	4 → 2	25.5	37.1	11.6
		Fe−O		
FeO	5 → 1	10.6	0.6	−10.0
Fe_2O_2	3 → 1	40.4	6.0	−34.4
FeO_2	3 → 1	26.4	8.0	−18.4
$Fe(O_2)^+$	4 → 2	47.1	14.0	−33.1
Fe_2O_4	3 → 1	7.0	0.7	−6.3

[a] For instance, 3 → 1 means that the energy of the singlet (low-spin) state relative to the triplet (high-spin) state.

an overall tendency in DFTB to overestimate the binding energies of low-spin complexes. Consequently, DFTB energetics should be carefully checked in the case of nickel parameters as well.

In Figure 5, as an example of a real case tier 4 system, structures and energetics of the intermediates of an ethylene insertion step of $[C_2H_4N_2NiCH_3]^+ + C_2H_4 \rightarrow [C_2H_4N_2NiCH_2CH_2CH_3]^+$ are presented. DFT geometries and energetics at the B3LYP/Lanl2DZ level were taken from ref 67. This system features Ni−H, Ni−C, and Ni−N interactions and similar trends as found for molecules in Table 15 can be observed. Ni−X bond lengths are generally too long by about 0.1 Å (with some exceptions). An exception is a very long agostic Ni···H distance of 2.72 Å for DFTB as compared to 2.15 Å for DFT the γ-complex; such a weak interaction does not seem to be properly parametrized. Energetically, DFTB interaction energies for π- and γ-complexes are in almost perfect agreement with DFT, but the β-complex is severely underbound relative to the γ-complex, which is in stark contrast to the DFT results. This finding underlines once again that energetics obtained at the DFTB level of theory are to be trusted only with great caution.

4. Sample Application in ONIOM(DFT:DFTB)

The deficiency in energetic prediction of spin-polarized DFTB with the present transition-metal parameters is expected to be greatly reduced in the ONIOM(QM:QM) scheme adopting DFTB as the low-level method. In this scheme the energetics of the "active" part will be calculated using a more reliable high-level method, and the energetic errors in the DFTB calculations will be mostly canceled out. The use of QM as the low-level method is in some cases essential; QM methods take into account electronic effects

Table 12. SDFTB and DFT (B3LYP/SDD+6-31G(d)) Optimized Bond Lengths (Å) and Valence Angles (°) of Co-Containing Tier 3 Molecules, for the Geometry Parameters Defined in Scheme 1

compound	multiplicity	parameter	DFT	SDFTB	Δ(DFTB−DFT)
		Co−H			
CoH	1	r	1.54	1.52	−0.02
	3	r	1.54	1.52	−0.02
CoH_2	2	r	1.49	1.47	−0.02
		α	97.4	93.9	−3.5
	4	r	1.59	1.58	−0.01
		α	143.2	140.3	−2.9
Co_2H_2	1	r	1.62	1.63	0.01
		α	48.4	47.1	−1.3
	3	r	1.63	1.64	0.01
		α	47.5	47.8	0.3
$Co(CH_3)_2$	2	r	1.89	1.99	0.10
		α	114.0	106.2	−7.8
	4	r	1.99	2.04	0.05
		α	143.9	146.8	2.9
$Co(C_2H_4)^{+2}$	4	r	2.30	2.08	−0.22
	6	r	2.19	2.06	−0.13
$CoCp^+$	4	r_1	1.80	1.79	−0.01
	6	r_1	2.30	2.52	0.22
		Co−N			
$Co(NH_2)_2$	4	r	1.82	1.80	−0.02
		α	179.9	179.4	−0.5
	6	r	1.90	1.84	−0.06
		α	97.0	96.3	−0.7
$Co(NH)_2$ linear	4	r	1.68	1.66	−0.02
		α	180.0	180.0	0.0
	6	r	1.78	1.73	−0.05
		α	179.1	180.0	0.9
$Co(NH)_2$ bent	4	r	1.67	1.65	−0.02
		α	128.4	127.0	1.4
	6	r	1.75	1.72	−0.03
		α	127.8	142.0	13.6
$Co^{2+}(\eta^1\text{-}N_2)$	2	r	2.00	1.95	−0.05
	4	r	1.99	1.98	−0.01
		Co−O			
CoO	2	r	1.60	1.58	−0.02
	4	r	1.59	1.61	0.02
Co_2O_2	1	r	1.73	1.77	0.04
		α	45.9	42.6	−3.3
	3	r	1.74	1.78	0.04
		α	44.2	45.1	0.9
CoO_2 linear	2	r	1.57	1.57	0.00
		α	177.7	179.5	1.8
CoO_2 bent	4	r	1.64	1.63	−0.01
		α	101.4	116.7	15.3
$Co(O_2)$	4	r	1.81	1.83	0.02
		α	47.9	44.7	3.2
	6	r	2.03	1.92	−0.11
		α	38.1	40.3	2.2
Co_2O_4	1	r_1	1.53	1.55	0.02
		r	1.75	1.78	0.03
		α	43.5	42.8	−0.7
	3	r_1	1.53	1.56	0.03
			1.76	1.78	0.02
		α	44.7	41.7	−3.0
	5	r_1	1.56	1.59	0.03
		r	1.75	1.78	0.03

Table 13. SDFTB and DFT (B3LYP/SDD+6-31G(d)) Dissociation Energies of Tier 3 Co-Containing Molecules

	dissociation energy (kcal/mol)		
dissociation process	DFT	DFTB	Δ(DFTB−DFT)
	Co−H		
$CoH_2(4) \rightarrow CoH(3) + H$	54.4	22.5	−31.9
$Co_2H(4) \rightarrow CoH(3) + Co(4)$	13.3	8.7	−4.6
	Co−C		
$CoC_2H_4^{+2} \rightarrow Co^{+2} + C_2H_4$	109.9	131.7	21.8
$Co(CH_3)_2(4) \rightarrow Co^{+2} + CH_3^-$	753.8	773.7	19.8
	Co−N		
$Co(NH_2)_2(4) \rightarrow Co^{+2} + 2NH_2^-$	386.2	430.2	45.0
	Co−O		
$CoO_2(2)$ bent $\rightarrow Co + O_2$	17.4	42.7	25.3
$Co(O_2)(2) \rightarrow Co + O_2$	10.4	23.0	12.6
$Co_2O_2(3) \rightarrow 2CoO$	21.5	52.7	31.2

Table 14. SDFTB and DFT (B3LYP/SDD+6-31G(d)) Energies (Relative to the Respective High-Spin States) of the Low-Lying Electronic States of Tier 3 Co-Containing Molecules

		relative energies (kcal/mol)		
compound	multiplicities[a]	DFT	SDFTB	Δ(DFTB−DFT)
	Co−H			
CoH	3 → 1	54.3	18.2	−36.1
CoH_2	4 → 2	11.2	−11.2	−22.4
Co_2H_2	3 → 1	25.3	10.5	−14.8
	Co−C			
$Co(CH_3)_2$	4 → 2	9.2	−1.1	−10.3
$Co(C_2H_4)^{+2}$	6 → 4	81.6	95.8	14.2
$CoCp^+$	6 → 4	21.8	46.0	24.2
	Co−N			
$Co(NH_2)_2$	6 → 4	−57.7	−74.0	−16.3
$Co(NH)_2$ bent	6 → 4	−8.8	−33.8	−25.0
$Co(NH)_2$ linear	6 → 4	6.7	49.0	42.3
$Co^{2+}(\eta^1\text{-}N_2)$	4 → 2	28.4	22.0	−6.4
	Co−O			
CoO	4 → 2	39.7	7.8	−31.9
Co_2O_2	3 → 1	5.3	1.1	−4.2
$Co(O_2)$	6 → 4	5.2	−26.8	−32.0
Co_2O_4	3 → 1	29.7	3.0	−26.7

[a] For instance, 3 → 1 means that the energy of the singlet (low-spin) state relative to the triplet (high-spin) state.

of the environment and are fully polarizable. Both of these important effects are neglected completely when standard MM is used as the low-level method. Since there is virtually no reliable semiempirical method for transition-metal complexes, even "preliminary" spin-polarized DFTB parameters would be useful for ONIOM(QM:QM) calculations.

To illustrate the applicability of the ONIOM(QM:DFTB) scheme, the approach is tested on a proposed mechanism for the iron enzyme isopenicillin N synthase.[30] This mechanism involves several metal oxidation and reduction steps, coupled to bond breaking and bond formation in the substrate. The range of different reactions makes it a suitable test system for ONIOM(QM:DFTB).

Table 15. SDFTB and DFT (B3LYP/SDD+6-31G(d)) Optimized Bond Lengths (Å) and Valence Angles (°) of Ni-Containing Tier 3 Molecules, for the Geometry Parameters Defined in Scheme 1

compound	multiplicity	parameter	DFT	SDFTB	Δ(DFTB−DFT)
		Ni−Ni			
$Ni_2(CH_3)_2$	1	r	2.19	2.22	0.03
		r_1	1.85	1.97	0.12
		α	97.3	96.9	−0.4
	3	r	2.35	2.16	−0.19
		r_1	1.91	2.01	0.10
		α	132.5	114.6	−17.9
$Ni_2(CH_3)_4$	1	r	2.46	2.24	−0.22
		r_1	1.86	1.98	0.12
		α	120.0	109.2	−10.8
	3	r	2.30	2.16	−0.14
		r_1	1.94	2.08	0.14
		r_2	1.91	2.08	0.17
		r_3	2.08	2.08	0.00
		α_1	121.0	114.1	−6.9
		α_2	121.1	114.1	−7.0
		α_3	60.1	114.1	54.0
		Ni−H			
NiH	2	r	1.51	1.46	−0.05
	4	r	1.60	1.60	0.00
NiH_2	1	r	1.53	1.54	0.00
		α	180.0	180.0	0.0
	3	r	1.54	1.52	−0.03
		α	131.9	136.8	4.9
Ni_2H_2	1	r	1.57	1.59	0.02
		α	41.4	45.1	3.3
	3	r	1.67	1.57	−0.10
		α	49.6	43.4	−6.2
		Ni−C			
$Ni(CH_3)_2^+$	1	r	1.94	2.04	0.10
		α	180.0	180.0	0.0
	3	r	1.96	2.03	0.06
		α	139.3	142.6	3.3
$Ni(C_2H_4)^+$	2	r	2.08	2.15	0.07
	4	r	2.32	2.28	−0.04
		r_1	2.85	3.08	0.23
$NiCp^+$	1	r_1	1.71	2.19	0.48
	3	r_1	1.77	1.90	0.13
		Ni−N			
$Ni(NH_2)_2^+$	2	r	1.88	1.81	−0.07
		α	176.5	180.0	3.6
	4	r	1.83	1.85	0.02
		α	180.0	180.0	0.0
$Ni(NH)_2$	1	r	1.60	1.66	0.06
		α	164.9	180.0	15.1
	3	r	1.67	1.72	0.05
		α	125.4	170.6	45.2
$Ni^+(\eta^1\text{-}N_2)$	2	r	1.91	1.94	0.03
	4	r	2.44	2.17	−0.27
		Ni−O			
NiO	1	r	1.61	1.62	0.01
	3	r	1.61	1.62	0.01
Ni_2O_2	1	r	1.75	1.79	0.04
		α	50.2	52.1	1.9
	3	r	1.77	1.78	0.01
		α	47.9	50.3	2.4
NiO_2	1	r	1.58	1.58	0.00
		α	159.4	180.0	30.6
	3	r	1.60	1.61	0.01

Table 15. (Continued)

compound	multiplicity	parameter	DFT	SDFTB	Δ(DFTB−DFT)
		α	132.7	142.0	10.7
$Ni(O_2)$	1	r	1.78	1.79	0.01
	3	r	1.90	1.83	−0.07
Ni_2O_4	1	r	1.76	1.78	0.02
		r_1	1.58	1.59	0.01
		α	42.7	41.2	−1.5

Table 16. SDFTB and DFT (B3LYP/SDD+6-31G(d)) Dissociation Energies of Tier 3 Ni-Containing Molecules

	dissociation energy (kcal/mol)		
dissociation process	DFT	DFTB	Δ(DFTB −DFT)
Ni−H			
Ni_2H_2 (3) → 2NiH (2)	38.9	−2.7	−41.6
Ni_2H_4 (1) → $2NiH_2$ (3)	30.3	8.1	−22.1
Ni−C			
$Ni(CH_3)_2$ (3) → Ni (3) + C_2H_6	5.4	14.5	9.1
$Ni(C_2H_4)^+$ (2) → Ni^+ (2) + C_2H_4	54.0	36.7	−17.3
$CpNi(C_2H_4)$ (2) → Ni (3) + Cp (2) + C_2H_4	71.4	39.5	−31.9
$NiCp^+$ (3) → Ni^+ (2) + Cp (2)	62.2	16.7	−45.5
Ni−N			
$Ni(NH_2)_2^+$ (2) → Ni^+ (2) + N_2H_4	66.4	73.3	6.8
$Ni(NH)_2$ (1) → Ni (3) + N_2H_2	120.5	136.5	16.0
$Ni^+(N_2)$ (2) → Ni^+ (2) + N_2	28.4	25.8	−2.7

Table 17. SDFTB and DFT (B3LYP/SDD+6-31G(d)) Energies (Relative to the Respective High-Spin States) of the Low-Lying Electronic States of Tier 3 Ni-Containing Molecules

		relative energies (kcal/mol)		
compound	multiplicities[a]	DFT	SDFTB	Δ(DFTB−DFT)
		Ni−Ni		
$Ni_2(CH_3)_2$	3 → 1	19.5	−3.8	−23.3
$Ni_2(CH_3)_4$	3 → 1	14.0	−8.4	−22.4
		Ni−H		
NiH	4 → 2	−26.3	−47.0	−20.7
NiH_2	3 → 1	33.8	12.0	−21.8
Ni_2H_2	3 → 1	28.6	−20.0	−48.6
		Ni−C		
$Ni(CH_3)_2^+$	3 → 1	35.9	10.4	−25.5
$Ni(C_2H_4)^+$	4 → 2	−39.9	−45.9	5.8
$NiCp^+$	3 → 1	21.2	−9.0	−30.2
		Ni−N		
$Ni(NH_2)_2^+$	4 → 2	10.4	−7.3	−17.7
$Ni(NH)_2$	3 → 1	−7.2	−29.6	−22.4
$Ni^+(\eta^1\text{-}N_2)$	4 → 2	−37.5	−57.0	−19.5
		Ni−O		
NiO	3 → 1	47.1	12.8	−34.3
Ni_2O_2	3 → 1	29.9	1.4	−28.5
NiO_2	3 → 1	2.7	−14.0	−16.7
$Ni(O_2)$	3 → 1	11.9	−10.7	−22.6

[a] For instance, 3 → 1 means that the energy of the singlet (low-spin) state relative to the triplet (high-spin) state.

All stationary points along the reaction coordinate are initially optimized at the B3LYP/6-31G(d) level. The relative B3LYP energies are also taken as target values for the lower-level calculations. ONIOM(B3LYP:DFTB) and DFTB-only energies are then obtained by performing single-point calculations on the DFT geometries. We used two ONIOM "models" to which the "high" level (DFT) is used, while the ONIOM "real" system is the full system, as shown at the bottom of Figure 6. The medium model is a model one would usually adopt in realistic calculations, while the small model is pushing the ONIOM a little further to check what the effect would be. Two resulting potential energy profiles (using medium and small models, respectively) are shown in the top row of Figure 6; due to technical issues with the preliminary ONIOM implementation, DFTB energies could not be properly converged for all stationary points, and those points have therefore been excluded from the results. Note also that the DFTB calculations use iron−sulfur parameters that are not included in the present contribution.

It takes only a brief look at Figure 6 to see that ONIOM-(DFT:DFTB) results are generally in very good agreement with those of the target DFT calculations. For the initial steps of the reaction, deviations between DFT and ONIOM results are in most cases limited to 1 kcal/mol. This accuracy is achieved despite the fact that relative DFTB errors are 10−20 kcal/mol, as could be expected from the data presented in previous sections. The higher accuracy of DFT:DFTB is achieved by the error cancellation that is an inherent part of the ONIOM method. The difference between DFT and DFT:DFTB results is larger for the last three stationary points in Figure 6, but only because these points describe bond breaking and formation directly adjacent to the DFTB layer. The apparent discrepancy can be removed by moving the cut between DFT and DFTB away from the reactive region.

The average absolute deviation for the ONIOM calculation using the medium model is 1.39 kcal/mol, excluding the reference and the last three stationary points. Including the last three points increases the deviation to 2.63 kcal/mol. Corresponding values for the DFTB calculation are 14.4 and 12.9 kcal/mol, respectively.

The present model was selected to show the applicability of the ONIOM(QM:DFTB) method rather than the potential benefits of an electronically active second layer. Still, the DFT:DFTB results are always better than the results from a small DFT model without the DFTB layer. The applicability and benefits of the present transition-metal parameters in ONIOM calculations will be further explored in subsequent work.

5. Summary and Conclusions

From the above given discussions in which geometries and energetics of tiers 3 and 4 molecules were presented for each transition-metal element at both the B3LYP/SDD+6-31G-(d) as well as spin-polarized DFTB level of theory, we can make the following summary:

1. Spin-polarized DFTB with the present parameters for transition-metal elements Sc, Ti, Fe, Co, and Ni in combination with H, C, O, N and same-element bonding partners reproduce B3LYP/SDD+6-31G(d) geometries reasonably well, both bond distances (average absolute differences mostly below 0.1 Å) as well as angles (average absolute deviations between 10° and 20°) except for cases where DFTB noticeably prefers linear bond environments, presumably as a consequence of the atomic DFTB parameter evaluation. Problems also occur in bonding situations where particular bond types were not included in tiers 1 and 2 molecule sets, such as metal−nonmetal π-bonds. A remedy of this problem would obviously involve the inclusion of π-complexes in tiers 1 and 2 sets of molecules; however, the overall DFTB performance for geometrical parameters is likely to suffer in such a case.

2. The evaluation of dissociation energies of these small molecules into even small molecular fragments (or sometimes atoms) is very difficult. The dissociation energies are only qualitatively acceptable. Some bonds are overbounds and some others underbound. Errors are as large as 4−50 kcal/mol is some cases.

3. For the energy differences between different spin states of tier 3 molecules, spin-polarized DFTB energetic orders qualitatively agree with DFT in most cases. However, for quantitative comparison, there are cases of both over- as well as underbinding by as much as 50 kcal/mol. While DFTB shows a tendency to overestimate the stability of low-spin complexes relative to their corresponding high-spin states, we found several exceptions to this rule. For tier 4 molecules, we also found both over- as well as underbinding situations of the order of tens of kcal/mol, making the use of DFTB predicted energetics only qualitative.

Therefore spin-polarized DFTB parameters for Sc, Ti, Fe, Ni, and Co in connection to H, C, N, O and own elements should be taken as "preliminary", with a reasonable geometrical performance but with only qualitative or "ballpark" energetic reliability and should be further tested for individual cases.

4. The deficiency in energetic prediction of spin-polarized DFTB with the present transition-metal parameters is expected to be greatly reduced in the ONIOM(QM:QM) scheme adopting DFTB as the low-level method. Since there is virtually no reliable semiempirical method for transition-metal complexes, even "preliminary" spin-polarized DFTB parameters would be useful for ONIOM(QM:QM) calculations. We have demonstrated using the proposed mechanism for the iron enzyme isopenicillin N synthase. The use of QM as the low-level method is in some cases essential; QM methods take into account electronic effects of the environment and are fully polarizable; both of these important effects are neglected completely when standard MM is used as the low-level method. The applicability of the present transition-metal parameters in the ONIOM(QM:DFTB) will be further explored in subsequent work.

In the present test, we used B3LYP/SDD+6-31G(d) for the calibration of the DFTB parameters. As is well-known, a weak point of the DFT method is the lack of an absolutely reliable functional. In particular, the amount of mixing of the "exact" (Hartree−Fock) exchange functional often controls the relative energies of different spin states. B3LYP has been used in the original parametrization of (H, C, N, O) set and is one of the most popular functionals in chemistry with a "somehow magic" hybrid ratio. Although in many cases such hybrid functionals with a small fraction of the exact exchange are known to give reasonable reaction energies and relative energies of different spin states,[68−71] there are many exceptions as well.[72] Therefore, if one tries to fit DFTB parameters to reproduce a different functional, one would result in a different parameter set.

The problems in predicting DFT-like energetics is partly stemming from the current fitting scheme for the diatomic pair repulsive curve and needs further improvement. Another problem of the present scheme of parameter determination is that one has to carefully work on each pair of elements, which is extremely time-consuming; with a few element pairs a year, it will be long before one can cover all the important element pairs. A more systematic method of determining parameters for a set of pairs of elements at the same time will be required. Efforts along these lines are in progress.

Acknowledgment. We would like to acknowledge Dr. David Quinonero for his participation in the early stage of this work. This work was supported in part by grants from the U.S. National Science Foundation (CHE-0209660), U.S. Department of Energy (DE-FG02-03ER15461), CREST (Core Research for Evolutional Science and Technology) in the Area of High Performance Computing for Multi-scale and Multi-physics Phenomena from the Japan Science and Technology Agency (J.S.T.), Deutsche Forschungsgemeinschaft (D.F.G.), and University of Paderborn. Computer resources were provided by the Cherry Emerson Center for Scientific Computation.

Supporting Information Available: Table S1−S5 and DFTB optimized Cartesian coordinates (in Å) (Sc, Ti, Fe, Ni, and Co compounds, respectively). This material is available free of charge via the Internet at http://pubs.acs.org.

References

(1) Hohenberg, P.; Kohn, W. *Phys. Rev.* **1964**, *136*, B864.

(2) Kohn, W.; Sham, L. J. *Phys. Rev.* **1965**, *140*, A1133.

(3) Parr, R. G.; Yang, W. *Density-Functional Theory of Atoms and Molecules*; Oxford University Press: New York, 1989.

(4) Dewar, M. J. S.; Thiel, W. *J. Am. Chem. Soc.* **1977**, *99*, 4899.

(5) Dewar, M. J. S.; Thiel, W. *J. Am. Chem. Soc.* **1977**, *99*, 4907.

(6) Nanda, D. N.; Jug, K. *Theor. Chim. Acta* **1980**, *57*, 95.

(7) Jug, K.; Iert, R.; Schulz, J. *Int. J. Quantum Chem.* **1987**, *32*, 265.

(8) Dewar, M. J. S.; Zoebisch, E.; Healy, E. F.; Stewart, J. J. P. *J. Am. Chem. Soc.* **1985**, *107*, 3902.

(9) Stewart, J. J. P. *J. Comput. Chem.* **1989**, *10*, 209.

(10) Stewart, J. J. P. *J. Comput. Chem.* **1989**, *10*, 221.

(11) Dewar, M. J. S.; Jie, C.; Yu, J. *Tetrahedron* **1993**, *49*, 5003.

(12) Holder, A. J.; Dennington, R. D.; Jie, C. *Tetrahedron* **1994**, *50*, 627.

(13) Thiel, W.; Voityuk, A. A. *Theor. Chim. Acta* **1992**, *81*, 391.

(14) Thiel, W.; Voityuk, A. A. *Theor. Chim. Acta* **1996**, *93*, 315.

(15) *SPARTAN. 4.0 ed*.; Wavefunction Inc.: Irvine, CA, 1995.

(16) Voityuk, A. A.; Zerner, M. C.; Rosch, N. *J. Phys. Chem. A* **1999**, *103*, 4553.

(17) Repasky, M. P. C., J.; Jorgensen, W. L. *J. Comput. Chem.* **2002**, *23*, 1601.

(18) Tubert-Brohman, v.; Guimarães, C. R. W.; Repasky, M. P.; Jorgensen, W. L. *J. Comput. Chem.* **2004**, *22*, 138.

(19) Tubert-Brohman, I.; Guimaraes, C. R. W.; Jorgensen, W. L. *J. Chem. Theory Comput.* **2005**, *1*, 817.

(20) Sattelmeyer, K. W.; Tirado-Rives, J.; Jorgensen, W. L. *J. Phys. Chem. A* **2006**, *110*, 13551.

(21) Sattelmeyer, K. W.; Tubert-Brohman, I.; Jorgensen, W. L. *J. Chem. Theory Comput.* **2006**, *2*, 413.

(22) Rocha, G. B.; Freire, R. O.; Simas, A. M.; Stewart, J. J. P. *J. Comput. Chem.* **2006**, *27*, 1101.

(23) Elstner, M.; Porezag, D.; Jungnickel, G.; Elsner, J.; Haugk, M.; Frauenheim, T.; Suhai, S.; Seifert, G. *Phys. Rev. B* **1998**, *58*, 7260.

(24) Porezag, D.; Frauenheim, T.; Köhler, T.; Seifert, G.; Kaschner, R. *Phys. Rev. B* **1995**, *51*, 12947.

(25) Zheng, G.; Irle, S.; Morokuma, K. *Chem. Phys. Lett.* **2005**, *412*, 210.

(26) Elstner, M.; Cui, Q.; Munih, P.; Kaxiras, E.; Frauenheim, T.; Karplus, M. *J. Comput. Chem.* **2003**, *24*, 565.

(27) Koskinen, P.; Häkkinen, H.; Seifert, G.; Sanna, S.; Frauenheim, T.; Moseler, M. *New J. Phys.* **2006**, *8*, 9.

(28) Zheng, G.; Irle, S.; Elstner, M.; Morokuma., K. *J. Phys. Chem. A* **2004**, *108*, 3128.

(29) Zheng, G.; Irle, S.; Morokuma, K. *J. Chem. Phys.* **2004**, *122*, 014708/1.

(30) Krüger, T.; Elstner, M.; Schiffels, P.; Frauenheim, T. *J. Chem. Phys.* **2005**, *122*, 114110.

(31) Zhou, H.; Tajkhorshid, E.; Frauenheim, T.; Suhai, S.; Elstner, M. *Chem. Phys.* **2002**, *277*, 91.

(32) Witek, H. A.; Irle, S.; Zheng, G.; Jong, W. A. d.; Morokuma, K. *J. Chem. Phys.* **2006**, *125*, 214706/1.

(33) Witek, H. A.; Morokuma, K.; Stradomska, A. *J. Theory Comput. Chem.* **2005**, *4*, 639.

(34) Witek, H. A.; Morokuma, K. *J. Comput. Chem.* **2004**, *25*, 1858.

(35) Witek, H. A.; Irle, S.; Morokuma, K. *J. Chem. Phys.* **2004**, *121*, 5163.

(36) Witek, H. A.; Morokuma, K.; Stradomska, A. *J. Chem. Phys.* **2004**, *121*, 5171.

(37) Małolepsza, E.; Witek, H. A.; Morokuma, K. *Chem. Phys. Lett.* **2005**, *412*, 237.

(38) Köhler, C.; Seifert, G.; Gerstmann, U.; Elstner, M.; Overhof, H.; Frauenheim, T. *Phys. Chem. Chem. Phys.* **2001**, *3*, 5109.

(39) Perdew, J. P.; Burke, K.; Ernzerhof, M. *Phys. Rev. Lett.* **1996**, *77*, 3865.

(40) Becke, A. D. *J. Chem. Phys.* **1993**, *98*, 5648.

(41) Lee, C.; Yang, W.; Parr, R. G. *Phys. Rev. B* **1988**, *37*, 785.

(42) Sarkar, P.; Springborg, M.; Seifert, G. *Chem. Phys. Lett.* **2005**, *405*, 103.

(43) Joswig, J.; Springborg, M.; Seifert, G. *J. Phys. Chem. B* **2000**, *104*, 2617.

(44) Seifert, G.; Terrones, H.; Terrones, M.; Jungnickel, G.; Frauenheim, T. *Solid State Commun.* **2000**, *114*, 245.

(45) Seifert, G.; Terrones, H.; Terrones, M.; Frauenheim, T. *Solid State Commun.* **2000**, *115*, 635.

(46) Seifert, G.; Tamuliene, J.; Gemming, S. *Comput. Mater. Sci.* **2006**, *35*, 316.

(47) Seifert, G.; Terrones, H.; Terrones, M.; Jungnickel, G.; Frauenheim, T. *Phys. Rev. Lett.* **2000**, *85*, 146.

(48) Ivanovskaya, V. V.; Heine, T.; Gemming, S.; Seifert, G. *Phys. Status Solidi B* **2006**, *243*, 1757.

(49) Köhler, C.; Seifert, G.; Frauenheim, T. *Comput. Mater. Sci.* **2006**, *35*, 297.

(50) Bertram, N.; Cordes, J.; Kim, Y. D.; Ganteför, G.; Gemming, S.; Seifert, G. *Chem. Phys. Lett.* **2006**, *418*, 36.

(51) Tamuliene, J.; Seifert, G. *Full. Nanot. Carbon Nanostruct.* **2005**, *13*, 279.

(52) Ivanovskaya, V. V.; Seifert, G.; Ivanovskii, A. L. *Semiconductors* **2005**, *39*, 1058.

(53) Enyashin, A.; Seifert, G. *Phys. Status Solidi B* **2005**, *242*, 1361.

(54) Kohler, C.; Seifert, G.; Frauenheim, T. *Chem. Phys.* **2005**, *309*, 23.

(55) Ivanovskaya, V.; Seifert, G. *Solid State Commun.* **2004**, *130*, 175.

(56) Krause, M.; Kuzmany, H.; Georgi, P.; Dunsch, L.; Vietze, K.; Seifert, G. *J. Chem. Phys.* **2001**, *115*, 6596.

(57) Münch, W.; Kreuera, K.-D.; Seifertb, G.; Maiera, J. *Solid State Ionics* **2000**, *136*, 183.

(58) Yang, M.; Jackson, K. A.; Koehler, C.; Frauenheim, T.; Jellinek, J. *J. Chem. Phys.* **2006**, *124*, 024308/1.

(59) Frauenheim, T.; Seifert, G.; Elsterner, M.; Hajnal, Z.; Jungnickel, G.; Porezag, D.; Suhai, S.; Scholz, R. *Phys. Status Solidi B* **2000**, *217*, 41.

(60) Kohler, C. Berucksichtigung von Spinpolarisationseffekten in einem dichtefunktionalbasierten Ansatz, Ph.D., University of Paderborn, 2004.

(61) Elstner, M.; Cui, Q.; Munih, P.; Kaxiras, E.; Frauenheim, T.; Karplus, M. *J. Comput. Chem.* **2002**, *24*, 565.

(62) Eschrig, H. *The Optimized LCAO Method and Electronic Structure of Extended Systems*; Akademieverlag: Berlin, 1988.

(63) Foulkes, W.; Haydock, R. *Phys. Rev. B* **1989**, *39*, 12520.

(64) Dolg, M.; Wedig, U.; Stoll, H.; Preuss, H. *J. Chem. Phys.* **1987**, *86*, 866.

(65) Wedig, U.; Dolg, M.; Stoll, H.; Preuss, H. In *Quantum Chemistry: The Challenge of Transition Metals and Coordination Chemistry*; Veillard, A., Ed.; Reidel: Dordrecht, 1986; p 79.

(66) Frisch, M. J.; Trucks, G. W.; Schlegel, H. B.; Scuseria, G. E.; Robb, M. A.; Cheeseman, J. R.; Montgomery, J. A., Jr.; T. V.; Kudin, K. N.; Burant, J. C.; Millam, J. M.; Iyengar, S. S.; Tomasi, J.; Barone, V.; Mennucci, B.; Cossi, M.; Scalmani, G.; Rega, N.; Petersson, G. A.; Nakatsuji, H.; Hada, M.; Ehara, M.; Toyota, K.; Fukuda, R.; Hasegawa, J.; Ishida, M.; Nakajima, T.; Honda, Y.; Kitao, O.; Nakai, H.; Klene, M.; Li, X.; Knox, J. E.; Hratchian, H. P.; Cross, J. B.; Bakken, V.; Adamo, C.; Jaramillo, J.; Gomperts, R.; Stratmann, R. E.; Yazyev, O.; Austin, A. J.; Cammi, R.; Pomelli, C.; Ochterski, J. W.; Ayala, P. Y.; Morokuma, K.; Voth, G. A.; Salvador, P.; Dannenberg, J. J.; Zakrzewski, V. G.; Dapprich, S.; Daniels, A. D.; Strain, M. C.; Farkas, O.; Malick, D. K.; Rabuck, A. D.; Raghavachari, K.; Foresman, J. B.; Ortiz, J. V.; Cui, Q.; Baboul, A. G.; Clifford, S.; Cioslowski, J.; Stefanov, B. B.; Liu, G.; Liashenko, A.; Piskorz, P.; Komaromi, I.; Martin, R. L.; Fox, D. J.; Keith, T.; Al-Laham, M. A.; Peng, C. Y.; Nanayakkara, A.; Challacombe, M.; Gill, P. M. W.; Johnson, B.; Chen, W.; Wong, M. W.; Gonzalez, C.; Pople, J. A. *Gaussian03 Rev. D01+*; 2004.

(67) Musaev, D. G.; Froese, R. D. J.; Svensson, M.; Morokuma, K. *J. Am. Chem. Soc.* **1997**, *119*, 367.

(68) Quiñonero, D.; Musaev, G. D. G.; Morokuma, M. *Inorg. Chem.* **2003**, *42*, 8449.

(69) Blomberg, M. R. A.; Siegbahn, P. E. M.; Svenson, M. *J. Chem. Phys.* **1996**, *104*, 9546.

(70) Lundberg, M.; Siegbahn, P. E. M. *J. Comput. Chem.* **2005**, *26*, 661.

(71) Ricca, A.; Bauschlicher, C. W. *J. Phys. Chem. A* **1997**, *101*, 8949.

(72) Jensen, K. P.; Roos, B. O.; Ryde, U. *J. Chem. Phys.* **2007**, *126*, 014103/1.

CT600312F